

# Investigating the *cis*-Regulatory Basis of C<sub>3</sub> and C<sub>4</sub> Photosynthesis in Grasses at Single-Cell Resolution

**John Pablo Mendieta<sup>1</sup>, Xiaoyu Tu<sup>2</sup>, Daiquan Jiang<sup>3</sup>, Haidong Yan<sup>1</sup>, Xuan Zhang<sup>1</sup>,  
Alexandre P. Marand<sup>1,4</sup>, Silin Zhong<sup>3</sup>, Robert J. Schmitz<sup>1,\*</sup>**

<sup>1</sup>Department of Genetics, University of Georgia

<sup>2</sup>Joint Center for Single Cell Biology, School of Agriculture and Biology, Shanghai Jiao Tong University, Shanghai 200240, China

<sup>3</sup>State Key Laboratory of Agrobiotechnology, School of Life Sciences, The Chinese University of Hong Kong

<sup>4</sup>Department of Molecular, Cellular, and Development Biology, University of Michigan

14

## 15 Abstract:

16  
17 While considerable knowledge exists about the enzymes pivotal for C<sub>4</sub> photosynthesis,  
18 much less is known about the *cis*-regulation important for specifying their expression in distinct  
19 cell types. Here, we use single-cell-indexed ATAC-seq to identify cell-type-specific accessible  
20 chromatin regions (ACRs) associated with C<sub>4</sub> enzymes for five different grass species. This  
21 study spans four C<sub>4</sub> species, covering three distinct photosynthetic subtypes: *Zea mays* and  
22 *Sorghum bicolor* (NADP-ME), *Panicum miliaceum* (NAD-ME), *Urochloa fusca* (PEPCK), along  
23 with the C<sub>3</sub> outgroup *Oryza sativa*. We studied the *cis*-regulatory landscape of enzymes  
24 essential across all C<sub>4</sub> species and those unique to C<sub>4</sub> subtypes, measuring cell-type-specific  
25 biases for C<sub>4</sub> enzymes using chromatin accessibility data. Integrating these data with  
26 phylogenetics revealed diverse co-option of gene family members between species,  
27 showcasing the various paths of C<sub>4</sub> evolution. Besides promoter proximal ACRs, we found that,  
28 on average, C<sub>4</sub> genes have two to three distal cell-type-specific ACRs, highlighting the  
29 complexity and divergent nature of C<sub>4</sub> evolution. Examining the evolutionary history of these  
30 cell-type-specific ACRs revealed a spectrum of conserved and novel ACRs, even among closely  
31 related species, indicating ongoing evolution of *cis*-regulation at these C<sub>4</sub> loci. This study  
32 illuminates the dynamic and complex nature of CRE evolution in C<sub>4</sub> photosynthesis, particularly  
33 highlighting the intricate *cis*-regulatory evolution of key loci. Our findings offer a valuable  
34 resource for future investigations, potentially aiding in the optimization of C<sub>3</sub> crop performance  
35 under changing climatic conditions.

36

## 37 Introduction:

38 Photosynthesis is one of the most critical chemical reactions on the planet whereby CO<sub>2</sub>  
39 is metabolized into glucose. Plants have evolved numerous variations of photosynthesis. The  
40 most common type of photosynthesis uses the enzyme ribulose 1,5-biphosphate carboxylase  
41 oxygenase (RuBisCO) which combines CO<sub>2</sub> with a five carbon compound ribulose 1,5-  
42 biphosphate to create 3-phosphoglyceric acid. This three-carbon compound is then used in a  
43 redox reaction within the Calvin Benson cycle, where sucrose is made. The production of this  
44 three-carbon compound is what gives this type of photosynthesis, C<sub>3</sub>, its name. However,  
45 although widely evolved and found in many crop plants, C<sub>3</sub> photosynthesis struggles to perform  
46 in hot, arid conditions. In non-ideal conditions, O<sub>2</sub> can competitively bind the RuBisCO active  
47 site, causing the formation of a toxic intermediate, and reducing photosynthetic efficiency and  
48 plant performance (1). Due to increasing temperature caused by anthropogenic climate change,  
49 this reduction in photosynthetic capacity for key crop plants poses a major agricultural challenge  
50 (2). However, other types of photosynthesis have evolved in hotter conditions and offer a model  
51 to potentially alter key C<sub>3</sub> crop plants to be more efficient.

52 The C<sub>4</sub> photosynthetic pathway is an example of a modified style of photosynthesis that  
53 is able to perform in hot conditions. In brief, C<sub>4</sub> typically works by sequestering key  
54 photosynthetic enzymes into two different compartments in the leaf made up of different cell  
55 types. These two cell types/compartments are bundle sheath (BS) cells, which in C<sub>4</sub> plants  
56 generally form a concentric ring around the vasculature, and mesophyll (MS) cells, which make  
57 up large portions of the non-vascularized leaf internal cells (3). In the MS, CO<sub>2</sub> is imported, and  
58 converted to bicarbonate (HCO<sub>3</sub><sup>-</sup>) by the enzyme carbonic anhydrase (CA). Bicarbonate is then  
59 converted to a four-carbon molecule oxaloacetate (OAA) by the O<sub>2</sub>-insensitive  
60 phosphoenolpyruvate carboxylase (PEPC). This OAA molecule made of a four-carbon  
61 compound (where C<sub>4</sub> derives its name) is finally converted into a stable metabolite, either  
62 malate or aspartate. This intermediate molecule is then transported to the BS where it  
63 undergoes a decarboxylation process, by one of three different types of decarboxylases, NAD-  
64 dependent malic enzyme (NAD-ME), NADP-dependent malic enzyme (NADP-ME), or  
65 phosphoenolpyruvate carboxykinase (PEPCK). This decarboxylation reaction releases a CO<sub>2</sub>  
66 molecule that enters into the Calvin Benson cycle. The generation and processing of  
67 intermediate molecules in cellular compartments allows for concentrated levels of CO<sub>2</sub> to  
68 interact with RuBisCO, reducing the inefficiencies mentioned above. Additional types of C<sub>4</sub>  
69 photosynthesis have been observed which don't rely on division of metabolites between MS and  
70 BS cell-types, but instead rely on using dimorphic chloroplast instead as in the species *Bienertia*  
71 *sinuspersici* (4,5). Current C<sub>4</sub> crops such as maize (*Zea mays*), sorghum (*Sorghum bicolor*),  
72 pearl millet (*Cenchrus americanus*), foxtail millet (*Setaria italica*), and broomcorn millet  
73 (*Panicum miliaceum*) excel in their ability to operate in adverse conditions.

74 Although the evolution of C<sub>4</sub> photosynthesis is a complex process, there is tantalizing  
75 evidence that engineering C<sub>3</sub> crops to do C<sub>4</sub> photosynthesis might be possible. One piece of  
76 evidence that points to this is that C<sub>4</sub> photosynthesis has evolved independently 65 times in  
77 different lineages of plants (6). These results indicate that most plant lineages have the genetic  
78 material capable of evolving into C<sub>4</sub> photosynthesizers. The Poaceae lineage of grasses  
79 exemplifies this, as C<sub>4</sub> photosynthesis has evolved independently at least 18 times (7).

80 Interestingly, all of these species use the same core C<sub>4</sub> enzymes and steps, but many use  
81 different decarboxylation enzymes as mentioned above (8–10). Furthering this hypothesis is the  
82 fact that many C<sub>4</sub> related genes originally evolved from either C<sub>3</sub> photosynthetic genes or key  
83 enzymes critical in core metabolism (11,12). For instance, PEPC is a key metabolism enzyme in  
84 the glycolytic pathways of the Krebs Cycle, with some copies being important in guard cell  
85 metabolism (13–15). Instead of novel gene content being the main driver of C<sub>4</sub> photosynthesis,  
86 it's more likely due to the correct timing and compartmentalization of key enzymes into specific  
87 cell types (16–18). This raises the question, how is gene expression of these key C<sub>4</sub> enzymes  
88 regulated? Moreover, as C<sub>4</sub> has evolved multiple times convergently, have similar regulatory  
89 networks and paradigms been co-opted to alter when and where these key genes are  
90 expressed?

91 *Cis*-regulatory elements (CREs) are key players in gene regulation, as they both fine  
92 tune expression and provide cell-type specificity (19–22). In brief, these regions operate as  
93 binding sites for transcription factors (TFs). Transcription factors are proteins which are able to  
94 alter transcription by binding DNA sequences and recruiting transcriptional machinery which  
95 can either increase or decrease transcription (23). Thus TFs are able to significantly change  
96 molecular phenotypes. Previous work has shown that CREs could be key players in the  
97 transition to C<sub>4</sub> photosynthesis. This was demonstrated by taking C<sub>4</sub> genes from *Z. mays* and  
98 transforming them into *Oryza sativa*, a C<sub>3</sub> species (24,25), which revealed that CREs from *Z. mays*  
99 genes were able to drive cell-type-specific expression in MS in *O. sativa* (24,25).  
100 Additional analyses have implicated CREs as drivers in the evolution of C<sub>4</sub> photosynthesis. In  
101 the genus of plants *Flaveria*, which contains both C<sub>4</sub> and C<sub>3</sub> plants, one key difference in C<sub>4</sub>  
102 plants was a specific CRE driving gene expression in MS cells. This 41 bp motif named  
103 *Mesophyll expression module 1* is critical for cell-type-specific expression of *PEPC* in MS cells,  
104 a critical first step in the C<sub>4</sub> pathway (19,26). Finally, four conserved non-coding sequences  
105 were identified to be critical in MS-specific expression of *PEPC* in monocots (27). Furthermore,  
106 a recent cross-species study examining the binding sites of GLK, a conserved TF regulating  
107 photosynthetic genes, revealed that CREs can undergo rapid changes and result in diverse  
108 gene expression patterns without the need of altering the TF itself (28). These findings show  
109 that CREs are important genetic elements that plants use for the evolution of C<sub>4</sub> photosynthesis.

110 Although some CREs critical for cell-type-specific expression of key photosynthetic  
111 genes have been identified, they've been restricted to those nearby the transcriptional start  
112 sites. This is due, in part, to the challenge of identifying CREs genome wide, as well as  
113 limitations in the isolation of BS and MS cells which is labor intensive and challenging. However,  
114 a recent study used a multi-omic approach in *Z. mays* BS and MS cells and found CREs  
115 genome-wide that might be critical in the cell-type-specific regulation of genes (29). One  
116 example is the identification of a potential distal CRE ~40 kb upstream of *SULFATE*  
117 *TRANSPORTER4* (*ZmSFP4*), a BS-specific sulfate transporter (29). These results highlight the  
118 complexity of identifying loci involved in *cis* regulation. Identifying all CREs associated with C<sub>4</sub>  
119 loci is critical in enhancing our understanding of *cis* regulation of key C<sub>4</sub> genes, and would  
120 greatly enhance attempts at engineering C<sub>3</sub> crops. During the evolution of C<sub>4</sub> photosynthesis, it's  
121 unclear whether these CREs have been pre-established during evolution and co-opted for C<sub>4</sub>  
122 photosynthesis or if they evolved independently numerous times. Understanding the ways in

123 which *cis* regulation evolves to control timing and cell-type-specific expression of C<sub>4</sub>  
124 photosynthesis genes would greatly assist efforts in engineering C<sub>3</sub> plants to be more C<sub>4</sub> like.

125 To investigate the role of CREs and their potential contribution in controlling key C<sub>4</sub>  
126 genes, we used single-cell indexed Assay for Transposase Accessible Chromatin sequencing  
127 (sciATAC-seq) to identify cell-type-specific CREs from five grass species representing diverse  
128 C<sub>4</sub> subtypes, as well as an additional C<sub>3</sub> outgroup. We investigated the cell-type specificity of  
129 both the core C<sub>4</sub> enzymes, and those which are unique to each photosynthetic subtype. Further,  
130 we identify CREs of C<sub>4</sub> genes, and find previously unknown cell-type-specific CREs that might  
131 be critical in C<sub>4</sub> gene expression. We find that some of these regulatory regions appear not just  
132 conserved in a single C<sub>4</sub> subtype, but in all of the C<sub>4</sub> species we studied. Finally, we leverage  
133 these data to find transcription factor binding motifs enriched in MS and BS cell types and use  
134 these motifs to catalog these regulatory loci.

135

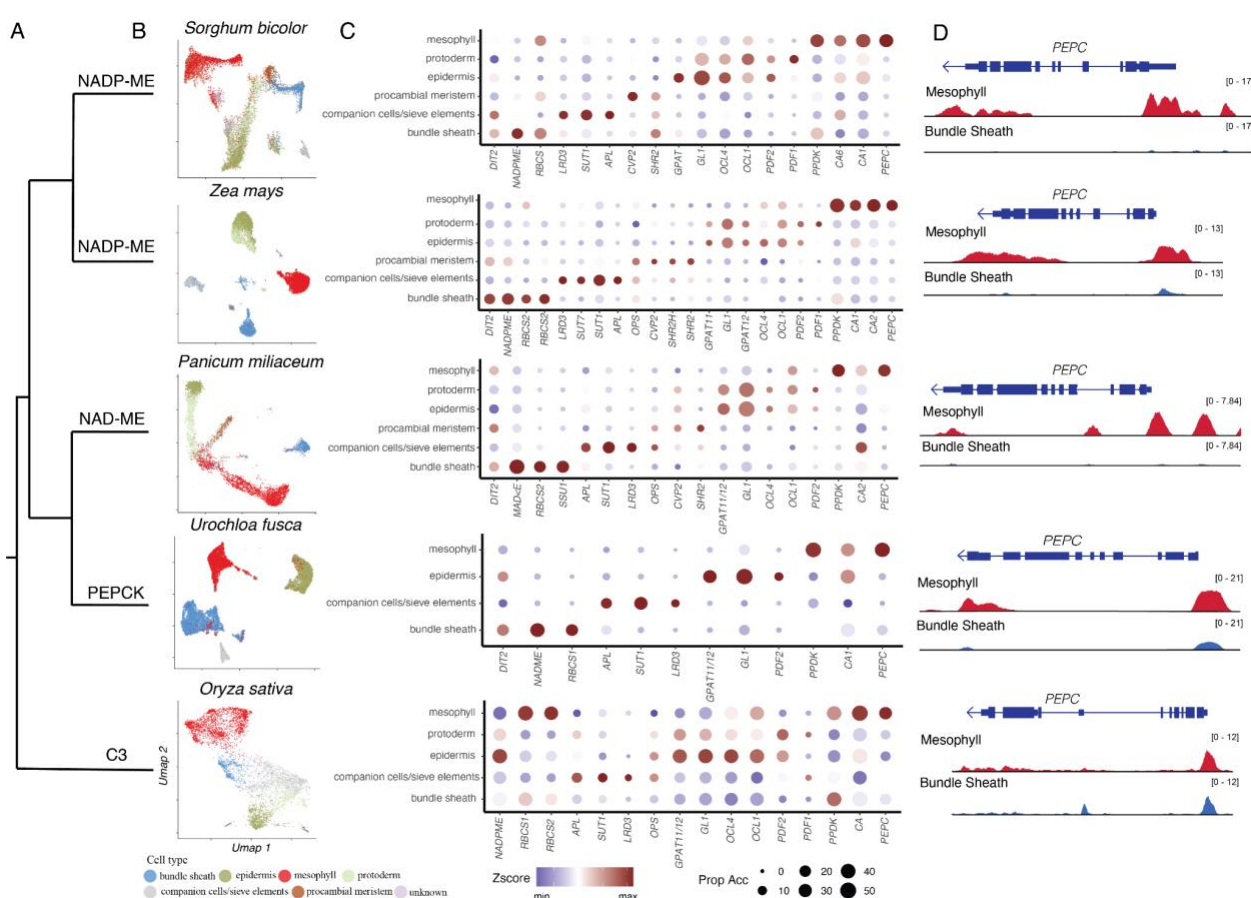
## 136 **Results:**

### 137 **Identification and Annotation of Cell Types in Diverse Species:**

138 To investigate CREs in BS and MS cells potentially important in C<sub>4</sub> photosynthesis, we  
139 generated replicated sciATAC-seq libraries for four different C<sub>4</sub> species, comprising three  
140 different C<sub>4</sub> subtypes NADP-ME (*Z. mays*, *S. bicolor*), NAD-ME (*Panicum miliaceum*), and  
141 PEPCK (*Urochloa fusca*), and a C<sub>3</sub> outgroup species (*O. sativa*) (**Figure 1A**). Libraries were  
142 filtered for high-quality cells by first pseudo-bulking the sciATAC-seq libraries, and identifying  
143 accessible chromatin regions (ACRs). Using these ACRs, per nuclei quality metrics were then  
144 calculated such as fraction of reads in peaks, transcriptional start site enrichment, and total  
145 integration events per nucleus (**Methods**). Nuclei found to have a high proportion of organellar  
146 reads were also removed, with values being adjusted on a per library basis (**Methods**).  
147 Clustering of cells was done on genomic bins, and with additional cells removed that had a high  
148 correlation with *in-silico* generated doublets, and clusters were removed that were skewed  
149 towards one replicate by greater than 75% (**Methods**). After filtering on per nucleus quality  
150 metrics, we identified 16,060 nuclei in *Z. mays*, 15,301 nuclei in *S. bicolor*, 7,081 nuclei in *P.*  
151 *miliaceum*, 19,110 nuclei in *U. fusca*, and 5,952 nuclei in *O. sativa* (**Supplemental Figure 1**,  
152 **Supplemental Table 1**).

153 Due to variation in genome size and content, cell-type annotation for each dataset was  
154 done independently using the reference genome for each species (**Figure 1B**). We used  
155 multiple approaches to annotate cell types. Orthologs of key marker genes from *Z. mays* and *O.*  
156 *sativa* were identified using a phylogenetics based approach (**Methods**). This allowed for the  
157 identification of marker genes for specific cell types in a cross species context. To gauge gene  
158 activity of these marker genes, gene body chromatin accessibility was used as a proxy for  
159 expression (**Figure 1D**) (21,30). Cell-type annotation was done manually taking into  
160 consideration marker gene chromatin accessibility, marker enrichment in clusters, as well as  
161 ontological relationships between cell types (**Supplemental Figure 2-19**). Due to the lack of  
162 marker genes for many cell types in plants, as well as the challenge of annotating a broad  
163 sample of species, we reduced resolution of our annotation across our datasets to ensure  
164 accurate comparisons between variable species (**Figure 1B**).

165 Deeper exploration of the list of marker genes from *Z. mays* showed conservation of  
 166 gene body chromatin accessibility in markers for certain cell types (**Supplemental Table 2-3**).  
 167 As expected, for the C<sub>4</sub> plants, *RIBULOSE BISPHOSPHATE CARBOXYLASE SMALL*  
 168 *SUBUNIT1 (RBCS1)* and *RIBULOSE BISPHOSPHATE CARBOXYLASE SMALL SUBUNIT2*  
 169 (*RBCS2*) were enriched in BS cells compared to MS cells (**Figure 1C**), a pattern that was not  
 170 found in *O. sativa*. Additionally, *PEPC1* showed MS-specific chromatin accessibility in all of the  
 171 C<sub>4</sub> species sampled (**Figure 1D**). Additionally, we found conservation of marker genes like  
 172 *SUCROSE TRANSPORTER 1 (SUT1)* in companion cells and sieve elements, and *GLOSSY1*  
 173 (*GL1*) in epidermis cells, indicating that these historically described marker genes are likely  
 174 important in this diverse set of species. This analysis provides a first examination of core-C<sub>4</sub>  
 175 marker genes' chromatin accessibility across a diverse sample of plant species at cell-type  
 176 resolution.  
 177



178  
 179 **Figure 1:** Annotation of cell types in diverse grass species at single-cell resolution **A)** A  
 180 phylogeny indicating the relationship of various C<sub>3</sub> and C<sub>4</sub> photosynthesizers sampled. In this  
 181 sample, two NADP-ME subtypes are represented, one NAD-ME subtype, a PEPCK subtype, as  
 182 well as a C<sub>3</sub> species. **B)** UMAP embedding showing the annotation for each species. A cell type  
 183 legend is below. **C)** Dotplots for various marker genes used to annotate each species. The y-  
 184 axis represents cell types, and the x-axis is a list marker genes used to annotate different cell  
 185 types. The size of each circle is proportional to the number of cells within that cell type that  
 186

187 showed chromatin accessibility of the marker. Color is z-score transformed values across  
188 clusters of gene chromatin accessibility across the clusters. **D)** Screenshots of the *PEPC* locus  
189 for all sampled species. For each screenshot, the top track shows the protein coding, the red  
190 track is chromatin accessibility of MS cells, and the blue track is the chromatin accessibility of  
191 the BS cells.

192

### 193 **Chromatin Accessibility of Core C<sub>4</sub> Enzymes Shows Similar Cell-Type Bias, but Differing** 194 **Evolutionary Origins:**

195 We measured the chromatin accessibility bias of the C<sub>4</sub>-associated enzymes. Due to the  
196 diverse nature of the plants sampled, and the C<sub>4</sub> photosynthetic subtypes, we separated  
197 enzymes into core- and subtype-specific groups. This list comprised nine core C<sub>4</sub> enzymes, and  
198 nine variable enzymes. These enzymes were assigned to one of these two groups based on if  
199 they are found in all C<sub>4</sub> subtypes (core) or are specific to only one or two subtypes (variable).  
200 One example of a core enzyme is carbonic anhydrase, which is used to generate bicarbonate  
201 from CO<sub>2</sub>, as well as for the regeneration of phosphoenolpyruvate from oxaloacetate in the BS  
202 cells by means of PEPCK (**Figure 2A**). The list of gene families that we considered as core or  
203 variable is found in (**Supplemental Table 4**).

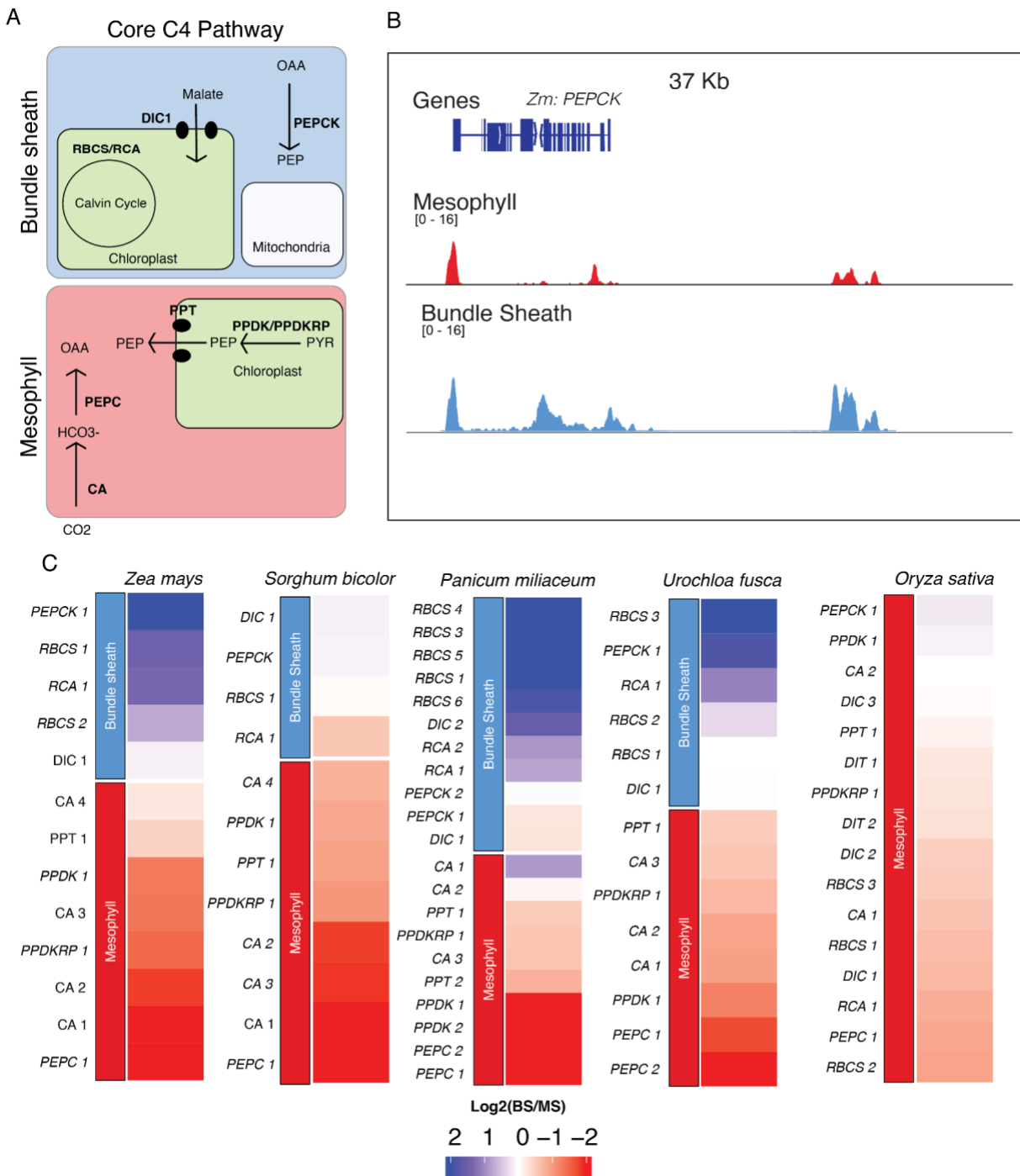
204 To investigate the cell-type bias of these enzymes, we used chromatin accessibility of  
205 the gene (gene body as well as 500 bp upstream of the transcriptional start site) (**Figure 2B**).  
206 Cell-type bias was calculated as the log<sub>2</sub> fold change of BS/MS chromatin accessibility. To  
207 identify core C<sub>4</sub> enzymes across these species, we used OrthoFinder, named and numbered the  
208 enzyme models based off of their relatedness to *Z. mays* copies of known core C<sub>4</sub> genes (31).  
209 Using only cell-type-specific chromatin accessibility data, we observed expected cell-type bias  
210 with many orthologs of the maize MS-specific core C<sub>4</sub> genes showing MS-specific bias as  
211 compared to BS (**Figure 2C**). For instance, in all C<sub>4</sub> species, *PEPCK*, which regenerates PEP  
212 from OAA in BS cells, always showed a BS-specific bias (**Figure 2 A & C**). Additionally, *PEPC*,  
213 which converts bicarbonate to OAA in MS cells, showed MS-specific bias for all species  
214 sampled, except the C<sub>3</sub> outgroup *O. sativa* (**Figure 2A & C**). These results highlight the quality  
215 of the data and the cell-type annotations for these single-cell datasets.

216 When analyzing these data in tandem with the phylogenetic trees, we noticed that some  
217 of the key enzymes showed different cell-type specificity based on their evolutionary origin  
218 (**Supplemental Figure 21-22**). For instance, for carbonic anhydrase in *P. miliaceum*, the  
219 orthologs that showed the largest bias between MS and BS cell types were not the copies that  
220 were the most evolutionary closely related to the *Z. mays* and *S. bicolor* cell-type-specific copies  
221 (Here *PmCA1* and *PmCA2*). Rather, a copy found in a separate clade (*PmCA3*) showed the  
222 most MS-specific bias (**Figure 2C**). This indicates that during the evolution of C<sub>4</sub>, different sets  
223 of carbonic anhydrases were likely co-opted for C<sub>4</sub>. One challenge using chromatin accessibility  
224 in this context, however, is the fact that neighboring gene models can occlude cell-type-specific  
225 signals. For instance, in the *S. bicolor* copy of *RBCS1*, a BS-specific gene has a neighboring  
226 gene model directly upstream which shares a promoter region making measurement of the cell-  
227 type-specific bias of some loci challenging when using chromatin accessibility data  
228 (**Supplemental Figure 23**).

229 One unexpected result from this analysis was the lack of cell-type-specific bias for  
230 *MALATE PHOSPHATE ANTIPORT 1 (DIC1)*, also known as

231 *DICARBOXYLATE/TRICARBOXYLATE TRANSPORTER 1 (DTC1)* in *Z. mays*. It has been  
232 previously reported that *DTC1* had BS-specific expression bias in *Z. mays* as well as in *P.*  
233 *miliaceum* (32–34). However, there is not a clear signal based on the chromatin accessibility  
234 data. This could indicate that some ACRs harbor multiple CREs active in different cell types that  
235 are not obvious in chromatin accessibility data or that the cell-type-specificity observed is not  
236 due to *cis*-regulation, possibly involving post-transcriptional processes (**Figure 2C**). Lastly, as  
237 expected, there was very little bias in the C<sub>3</sub> outgroup (*O. sativa*). In total, 12/13 of the core C<sub>4</sub>  
238 enzymes showed cell-type-specific bias in *Z. mays*, 7/12 in *S. bicolor*, 16/21 in *P. miliaceum*,  
239 11/13 in *U. fusca*, and finally 0/16 in *O. sativa*. These data demonstrate that chromatin-  
240 accessibility data can be leveraged to investigate the cell-type regulation of C<sub>4</sub> genes while also  
241 taking into consideration their evolutionary relationships in a cross species context.

242  
243  
244  
245  
246



247  
248

249 **Figure 2:** Cell-type chromatin-accessibility bias for core enzymes in C<sub>4</sub> and C<sub>3</sub> species. **A)**  
250 Schematic of the core C<sub>4</sub> enzymatic pathway. Core C<sub>4</sub> enzymes are defined as those which  
251 maintain their cell-type-specificity in all C<sub>4</sub> subtypes sampled. The red and blue squares  
252 represent MS and BS cells, respectively. Enzymes are labeled in bold, and transporters are  
253 denoted by shapes. Intermediate molecules are indicated by non-bolded text. **B)** Screenshot of  
254 *PEPCK* in *Z. mays*. Blue tracks correspond to BS chromatin accessibility and red tracks show  
255 MS chromatin accessibility. Tracks are equally scaled to facilitate comparison. **C)** Heatmaps of

256 chromatin accessibility bias of the core C<sub>4</sub> enzymes. Values within each heatmap correspond to  
257 Log2(BS/MS). Blue indicates increased BS chromatin accessibility and red indicates increased  
258 MS chromatin accessibility. Each species column and subtype was clustered independently,  
259 and genes were assigned as being MS- or BS-specific (top/bottom of heatmap) based on  
260 literature. Enzyme copies were distinguished phylogenetically.  
261

## 262 **Key C<sub>4</sub> Subtype Enzymes Show Potential Convergent Evolution in Cell-type-specific 263 Bias:**

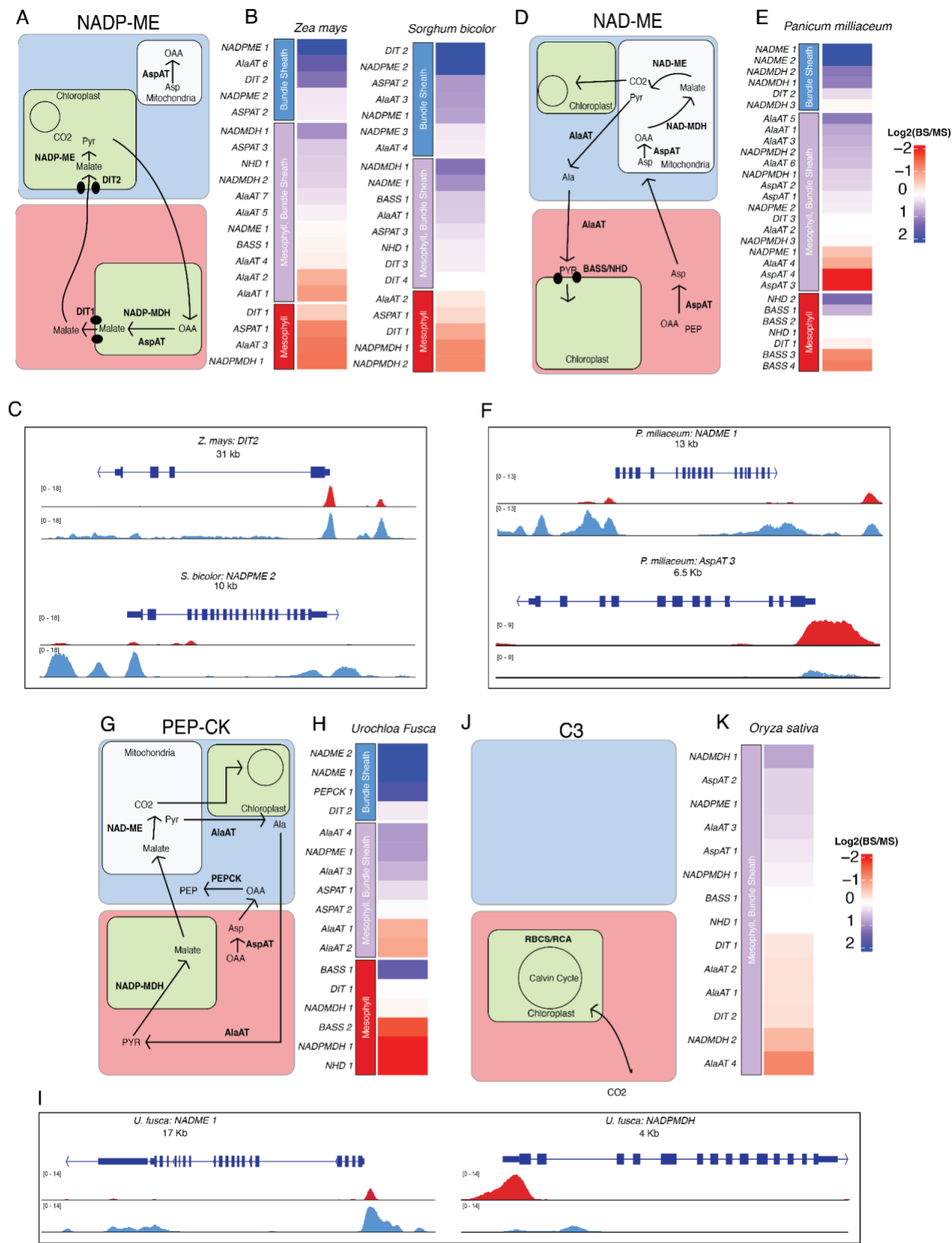
264 We investigated the variable enzymes that give each C<sub>4</sub> subtype its unique properties by  
265 focusing on two species (*S. bicolor* and *Z. mays*) from the *NADP-ME* subtype (**Figure 3A**). As  
266 expected, chromatin accessibility bias was observed for enzymes previously reported as having  
267 cell-type-specific expression patterns, similarly to the core C<sub>4</sub> enzyme set (29,35). Reassuringly,  
268 one of the most biased enzymes identified was *NADP-ME*, the key enzyme of the redox step in  
269 *NADP-ME* subtypes. More specifically, of the multiple copies of *NADP-ME* that exist in *Z. mays*,  
270 we observed the expected cell-type bias for the known BS-specific copy, *ME3*, a key factor in C<sub>4</sub>  
271 (here *ZmNADP-ME1*) (**Figure 3B**). We noticed in *S. bicolor*, the BS-specific *NADP-ME* and the  
272 MS-specific *NADP-malate dehydrogenase* (*NADP-MDH*) gene copies are recent tandem  
273 duplications, each maintaining their respective cell-type specific chromatin accessibility (**Figure**  
274 **3B & C, Supplemental Figure 22**). The malate transporters *DICARBOXYLIC ACID*  
275 *TRANSPORTER1/2* (*DIT1/2*) also demonstrated their expected cell-type-specific bias with *DIT1*  
276 being MS specific and *DIT2* being BS specific in both species (**Figure 3B & C**). However, upon  
277 further inspection of the phylogenies of the *DITs* in *S. bicolor*, we noticed a pattern where the  
278 most BS-biased copy, *SbDIT4* (Sobic.004G035500), was phylogenetically more closely related  
279 to the *ZmDIT1*. Something which has been previously reported (33,36). These results indicate  
280 that over evolutionary time, even members of the same C<sub>4</sub> photosynthetic subtype, which likely  
281 share a C<sub>4</sub> ancestor, can use different paralogous loci to achieve cell-type-specific expression.  
282 This highlights that C<sub>4</sub> evolution is an ongoing process.

283 NAD-ME subtypes in *P. miliaceum* are interesting, as the intermediate molecule being  
284 passed between MS and BS doesn't take the form of malate, but instead aspartate, alanine, and  
285 oxaloacetate (**Figure 3D**). At least one copy of all of the key redox enzymes, NAD-ME and the  
286 NAD-dependent malate dehydrogenase (NAD-MDH), show BS-biased chromatin accessibility  
287 (**Figure 3E & F**). Interestingly, of the three copies of *NAD-MDH* analyzed, only two showed bias  
288 for BS. Next, we evaluated two key enzymes associated with the generation of critical  
289 intermediate metabolites, Aspartate aminotransferase (AspAT), and Alanine aminotransferase  
290 (AlaAT). It has been reported that some AspAT have cell-type-specific expression patterns, with  
291 the MS-specific copy of the protein being transported to the cytosol and the BS-specific copy  
292 being transported to the mitochondria (**Figure 3E & F**) (37–39). Of the four copies of AspAT we  
293 examined, two (*PmAspAT3/4*) showed significant MS-specific bias, whereas the other two  
294 copies (*PmAspAT1/2*) didn't show significant deviation towards BS (**Figure 3E**). This possibly  
295 indicates differing levels of regulation for the AspAT copies that did not show the expected BS  
296 bias, or missing copies of AspAT that we have not investigated. Within AlaAT, however, we  
297 identified one copy, *PmAaAT1*, showing MS-specific bias, and *PmAaAT6* showing BS-specific  
298 bias; something that has been previously hypothesized based on biochemical information (40).  
299 Additionally, somewhat unexpectedly is that we didn't observe clear bias for sodium bile acid

300 symporters (*BASS*) and sodium:hydrogen antiporters (*NHD*) (**Figure 3E**). These two proteins  
301 together form a functioning sodium bile acid symporter system, which balances the ratio of  
302 sodium and is important in the transport of pyruvate into the chloroplast of MS cells (41).  
303 Although two copies of the *BASS* genes were MS biased, only a single copy of *NHD* was  
304 slightly MS biased. Surprisingly, we do observe slight cell-type-specific chromatin accessibility  
305 bias for malate transporter *DIT1/DIT2* in *P. miliaceum*. This is somewhat surprising, as malate is  
306 not the main 4-carbon intermediate used by NADP-ME subtypes (10). This highlights the flexible  
307 nature of *P. miliaceum* in terms of its C<sub>4</sub> photosynthetic style, as it has been implicated that it  
308 can perform some of the metabolite shuttling as the NADP-ME subtype (10,42,43). The  
309 potential flexibility of *P. miliaceum* in its style of C<sub>4</sub> makes it an extremely interesting species to  
310 study, especially when considering that it doesn't share common C<sub>4</sub> ancestry with *Z. mays* or *S. bicolor*. This lack of evolutionary relationship between *P. miliaceum* and *S. bicolor* and *Z. mays*  
311 makes the comparison between *P. miliaceum* and its closer relative *U. fusca* all the more  
312 valuable. These observations point to the complicated nature of some of these C<sub>4</sub>  
313 photosynthetic subtypes. While the obvious subtype-specific enzymes show expected  
314 chromatin-accessibility bias, others do not.  
315

316 Using the *PEPCK* subtype in *U. fusca*, we evaluated cell-type bias of enzymes that  
317 operate as an intermediate between NAD-ME and NADP-ME subtypes (**Figure 3G**). Copies of  
318 *NAD-ME* and *PEPCK* showed significant BS bias (**Figure 3H & I**). Additionally, *NADP-MDH* was  
319 significantly biased towards MS, reflecting its critical role in the regeneration of malate from  
320 pyruvate (**Figure 3H**). We also observed one copy of *BASS*, which was heavily MS biased, as  
321 well as the only copy of *NHD* being highly MS biased (**Figure 3G**) (44). Within the *BASS* family,  
322 based on the phylogenies, it appears one clade of *BASS* genes was co-opted to be MS specific,  
323 whereas the other clade remained somewhat BS specific. This potentially indicates that this co-  
324 opted clade may have been predisposed for C<sub>4</sub> photosynthesis at the common ancestor of *P.*  
325 *miliaceum* and *U. fusca*. Additionally, we also find one MS-biased and one BS-biased version of  
326 *AlaAT* (**Figure 3H**).  
327

328 Finally, when evaluating genes in the C<sub>3</sub> outgroup *O. sativa*, we only observed significant  
329 chromatin accessibility bias for three of the 14 enzymes. This is expected given the overall lack  
330 of enzymatic bias seen in C<sub>3</sub> species (**Figure 3K**). Interestingly though, we did find a single  
331 instance where one copy of *AspAT* is BS specific, suggesting that this copy of *AspAT* might  
332 slowly be co-opted into being more BS-specific (**Figure 3K**). Even more interesting is the slight  
333 BS-specific bias of the rice *NAD-MDH*, a BS-specific enzyme in the *NAD-ME* subtypes. These  
334 results show a series of complex evolutionary relationships where many different genes can be  
335 co-opted into the C<sub>4</sub> pathway, and highlights the myriad ways in which C<sub>4</sub> evolution occurs.  
336  
337



341 blue squares represent MS and BS cells. Enzymes are labeled in bold, and transporters are  
342 denoted by shapes. Intermediate molecules are indicated by non-bolded text. For clarity, core  
343 enzymes have been removed. **B/E/H/K**) Heatmaps of chromatin accessibility bias in C<sub>4</sub> subtype  
344 enzymes. Values within the heatmap correspond to Log2(BS/MS). Blue indicates increased BS-  
345 chromatin accessibility and red indicates increased MS-chromatin accessibility. Genes were  
346 labeled as being BS specific (blue) BS/MS specific (purple) or MS specific (red) based on  
347 previous literature. **C/F/I**) Screenshot of various C<sub>4</sub> sub-type enzymes and their chromatin  
348 accessibility profiles around the TSS. Blue tracks correspond to BS chromatin accessibility and  
349 red tracks show MS chromatin accessibility. Tracks are equally scaled to facilitate comparison.  
350

351 **Cell-type-specific Accessible Chromatin Regions of Both Core- and Subtype-Specific**  
352 **Enzymes:**

353 Although measuring the gene body chromatin accessibility of C<sub>4</sub> enzymes is valuable, it  
354 doesn't inform us about the cell-type-specific *cis*-regulatory environment controlling these  
355 genes, as we only included 500 bp upstream in this initial analysis. To identify all potential CREs  
356 important for regulation of C<sub>4</sub> enzymes, we identified cell-type-specific ACRs using a modified  
357 entropy metric (**Methods; Supplemental Figure 33-34**). In short, cell-type-specific ACRs are  
358 those which are unique to either a single cell-type or two or three cell-types in contrast to  
359 broadly accessible ACRs which are accessible in many different cell-types. For each C<sub>4</sub>  
360 enzyme, in both the core and the non-core set, we identified ACRs around them. We only  
361 considered ACRs to be potential regulators of a locus based on distance, with assigned ACRs  
362 needing to be less than 200 kb away from the target enzyme, and requiring that no other gene  
363 intervenes between the ACR and enzyme in question. In total, across all variable and core  
364 enzymes and taking into consideration only C<sub>4</sub> species, we find that on average, C<sub>4</sub> genes have  
365 between 2-3 cell-type-specific ACRs, with an additional 2-3 broadly-accessible ACRs (**Figure**  
366 **4A, Supplemental Table 5**).

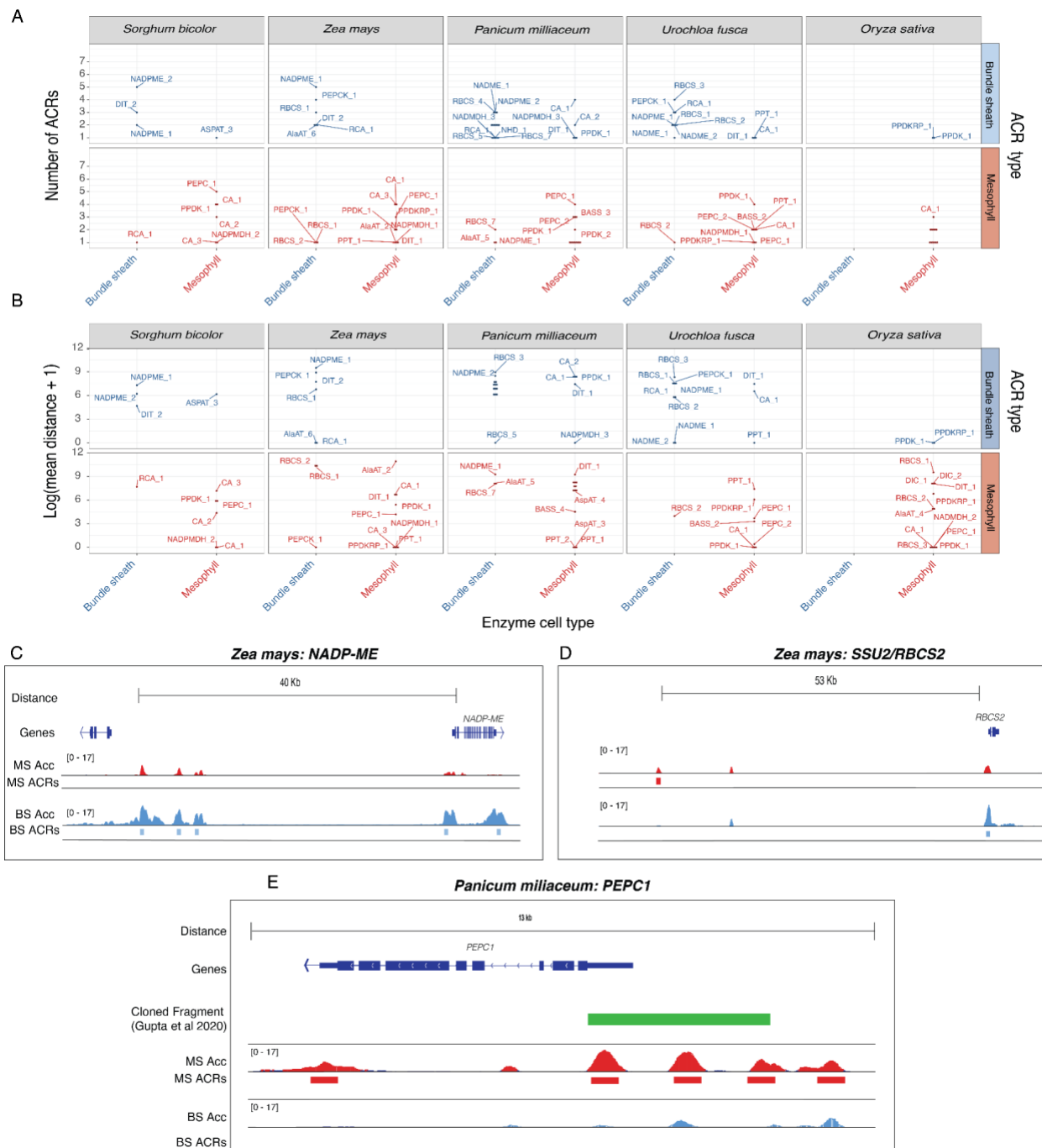
367 For all C<sub>4</sub> subtypes, the key redox enzymes all showed BS cell-type-specific ACRs,  
368 potentially identifying critical CREs for proper cell-type-specific expression. For instance, in *Z.*  
369 *mays*, *NADP-ME1* had five BS-specific ACRs, in *S. bicolor*, *NADP-ME2* had five BS-specific  
370 ACRs, in *P. miliaceum*, *NAD-ME1* had four BS-specific ACRs, and in *U. fusca*, *PEPCK*, had  
371 three BS-specific ACRs (**Figure 4 A & C**). Additionally, of the MS-specific enzymes, we  
372 consistently observed numerous cell-type-specific ACRs around the carbonic anhydrase family.  
373 On average, there were 3.5 MS-specific ACRs for each copy of carbonic anhydrase across all of  
374 the species. This likely reflects the fact that carbonic anhydrase is critical in the initial steps of  
375 C<sub>4</sub>, and also important in CO<sub>2</sub> sensing (45). We also noticed an intriguing pattern where  
376 enzymes which were accessible in one cell type had cell-type-specific ACRs of the other cell  
377 type. For instance, around *RBCS2*, a BS-specific enzyme, we found a series of MS-specific  
378 ACRs (**Figure 4D**). On average, we found 2.5 BS-specific ACRs around *RBCS* and 1.5 MS-  
379 specific ACRs. This contrasting pattern was observed in key photosynthetic enzymes in all of  
380 the C<sub>4</sub> subtypes. This likely indicates that some of these ACRs contain CREs that negatively  
381 regulate *RBCS* in MS, as cell-type-specific CRE usage has been implicated as being an  
382 important driver in proper compartmentalization (46,47). The identification of ACRs around key  
383 C<sub>4</sub> enzymes provides a detailed map about potential *cis*-regulators of these loci, which provides  
384 the basis for future investigation into the direct function of each of these ACRs and how they

385 might be altering transcription in multiple different ways. These results show that there are likely  
386 multiple ACRs important to cell-type specificity of these enzymes.

387 Traditionally, the field has focused on *cis*-regulation within a set distance from the  
388 transcriptional start site, often 1-2 kb, which is thought to generally encompass the promoter  
389 (48). However, we observed abundant distal cell-type-specific ACRs for many of these key  
390 genes (**Figure 4B**). For instance, the average distance of an ACR to its C<sub>4</sub> enzyme is 10,080 bp  
391 (*Z. mays*), 3,017 bp (*S. bicolor*), 4,260 bp (*P. miliaceum*), 2,358 bp (*U. fusca*), and 4,730 bp (*O.*  
392 *sativa*), indicating that the *cis*-regulatory space for these enzymes is far greater than previously  
393 appreciated, where a majority of the focus in the literature is on putative promoters. To test this,  
394 we compared the identified ACRs to a series of previously reported cloned promoters. We found  
395 that for *Zea mays* and *Sorghum bicolor* the ACR space identified includes significantly more  
396 regions that are distal to their target gene (**Supplemental Figure 23C, Supplemental Table 6**)  
397 (25,49,50).

398 The genome of *Z. mays* emphasizes this point, as the subtype-specific enzyme *NADP-ME* has  
399 three cell-type-specific BS ACRs distal to the transcriptional start site, with the furthest being  
400 34,336 bp away (**Figure 4C**). These distal ACRs provide critical regulatory loci to further  
401 investigate. Interestingly, we found some enzyme/ACR pairs with opposite cell-type-specificity  
402 (*i.e.* BS-specific enzyme, MS-specific ACR). Many of these ACRs were distally located. For  
403 example, in *Z. mays*, the MS-specific ACR of *RBCS* was 36,171 bp upstream (**Figure 4D**).  
404 When investigating ACRs around promoters, we were struck at how often cell-type-specific  
405 ACRs occurred outside of the bounds of previously analyzed promoters. For example, in *PEPC*  
406 in *P. miliaceum*, a recent analysis demonstrated that a series of conserved non-coding  
407 sequences found between species were able to drive MS expression (27). When we looked at  
408 chromatin accessibility data of the promoter fragment which was cloned from *PEPC*, we  
409 identified many MS-specific ACRs within the cloned fragment, but an additional one upstream.  
410 This results shows the advantage of using scATAC-seq data to identify candidate CREs for  
411 certain genes, removing the guesswork of cloning fragments to investigate and providing a  
412 detailed cell-type-specific regulatory map of the locus (**Figure 4E**). Thus, scATAC-seq greatly  
413 improves the search space of the active CREs potentially driving cell-type-specific gene  
414 expression patterns.

415



416  
417  
418  
419  
420  
421  
422  
423  
424  
425

**Figure 4: Investigating the number and distance of cell-type-specific ACRs around C<sub>4</sub> enzymes across subtypes. A)** Dot plots showing the number of cell-type-specific ACRs around each enzyme. The x-axis indicates which cell type these enzymes are found in. The y-axis is counts of ACRs. The graph is further subdivided with the top panel being broad ACRs, middle panel BS-specific ACRs, and the bottom being MS-specific ACRs. Enzymes are labeled. **B)** Dotplots showing the mean distance of cell-type-specific ACRs to their closest C<sub>4</sub> enzyme. The x-axis is the genomic distance to the C<sub>4</sub> enzyme in question. If an enzyme had multiple cell-type-specific ACRs, the distance was averaged (mean). **C)** Screenshot of NADP-ME1 in *Z. mays*. Blue tracks correspond to BS

426 chromatin accessibility and red tracks show MS chromatin accessibility. Tracks are equally  
427 scaled to facilitate comparison. All genes found within this window are shown. **D)** Screenshot of  
428 *RBCS2* in *Z. mays*. Blue tracks correspond to BS chromatin accessibility and red tracks show  
429 MS chromatin accessibility. Tracks are equally scaled to facilitate comparison. All genes found  
430 within this window are shown. **E)** Screenshot of *PEPC1* in *P. miliaceum*. The green fragment  
431 represents the cloned promoter from Gupta et al 2020, which was identified by minimap2  
432 alignment. Blue tracks correspond to BS chromatin accessibility and red tracks show MS  
433 chromatin accessibility. Tracks are equally scaled to facilitate comparisons.

434

435 **The Evolutionary Relationships of ACRs Associated with C<sub>4</sub> Genes is Complex and**  
436 **Variable:**

437 Next, we explored the evolutionary histories of these ACRs. Due to the fact that the C<sub>4</sub>  
438 subtypes come from different radiation events, (with *Z. mays* and *S. bicolor* likely sharing a C<sub>4</sub>  
439 ancestor and *U. fusca* and *P. miliaceum* sharing a different C<sub>4</sub> ancestor), we were curious to  
440 evaluate if a majority of the ACR space around these genes were either novel, or shared among  
441 these species. We implemented a pairwise sequence based approach by identifying sequence  
442 conservation of ACRs between the study species using BLAST (**Methods**). The majority of  
443 important C<sub>4</sub> genes have both novel, and conserved ACRs. For example, PPDK, a MS-specific  
444 enzyme, shares ~25% of its ACRs across all species examined including the *O. sativa* C<sub>3</sub>  
445 outgroup (**Figure 5A**). Interestingly, *RUBISCO ACTIVASE* (RCA), a critical enzyme in  
446 photosynthesis which removes inhibitory molecules from the RuBisCO active site, had novel  
447 ACRs in all of the C<sub>4</sub> species examined, whereas RCA in the C<sub>3</sub> species *O. sativa* shared one  
448 ACR with all of the C<sub>4</sub> species. This might indicate that each of the C<sub>4</sub> species gained regulatory  
449 sequences at RCA or that *O. sativa* might have lost them (**Figure 5A**). Focusing on NADP-ME  
450 revealed notable divergence in its associated ACRs, even among closely related species. For  
451 example, in *Z. mays*, two out of nine ACRs linked to *NADP-ME1* were unique, lacking  
452 counterparts in other species (**Figure 5A**). This is particularly striking given that *S. bicolor*,  
453 belonging to the same C<sub>4</sub> subtype, diverged from *Z. mays* only 13 million years ago (51).  
454 Similarly, in *S. bicolor*, the BS-specific *NADP-ME2* variant exhibited two out of five unique  
455 ACRs. This pattern underscores the rapid and distinct evolutionary trajectories of ACRs in C<sub>4</sub>  
456 plants. A full list of gene families, and gene models, and their relative conservation is found in  
457 **Supplemental Figure 25A**. Using this same approach to study all of the core class of C<sub>4</sub>  
458 enzymes did not reveal a generalizable pattern associated with gain or loss of ACRs around C<sub>4</sub>  
459 genes (**Supplemental Figure 25A**). Our findings not only confirm the dynamic evolution of *cis*-  
460 regulatory sequences in C<sub>4</sub> enzymes but also align with existing research that highlights rapid  
461 *cis*-regulatory changes among closely related species (48,52).

462 While investigating the ACRs around the C<sub>4</sub> genes is interesting, understanding how  
463 cell-type specificity is achieved across C<sub>4</sub> subtypes is needed for efforts to engineer C<sub>4</sub>  
464 photosynthesis. When looking at just the cell-type-specific ACRs around key C<sub>4</sub> loci, we find a  
465 similar pattern where there is a mix of both conserved and novel ACRs. For example, we  
466 discovered that some of the MS-specific ACRs associated with *PPDK* and *PEPC* are highly  
467 conserved in all of the studied species. Interestingly, the MS-specific ACRs around *PEPC* were  
468 only found in the C<sub>4</sub> species, and not in the C<sub>3</sub> outgroup, *O. sativa* (**Figure 5B**). This indicates

469 that some of the CREs that allow *PEPC* expression in MS likely evolved after the split between  
470 the most recent common ancestors. We also observed that *NADP-ME* possessed numerous  
471 BS-specific ACRs that were conserved in all species, including *O. sativa* (**Figure 5B**).  
472 Considering the fact that proper compartmentalization of *NADP-ME* in BS cells is only critical in  
473 two of the three  $C_4$  subtypes, this was surprising. However, in both *S. bicolor* and *Z. mays*, there  
474 were novel BS-specific ACRs associated with each key *NADP-ME*. In *Z. mays*, one out of the  
475 five BS-specific ACRs was novel to *Z. mays*, and in *S. bicolor* two out of the five were novel to  
476 *S. bicolor*. Upon inspection of all the *NADP-ME* loci in genome browsers, we were struck by the  
477 complexities and shuffling that occurred at these BS cell-type-specific ACRs (**Figure 5C**). These  
478 results highlight that extensive *cis*-regulatory evolution is occurring in each of these species,  
479 and in particular on a cell-type-specific level. Additionally, this may point to the fact that the  
480 novel BS-specific ACRs found in *S. bicolor* and *Z. mays* may be more important for proper BS-  
481 specific expression than the conserved regulatory elements.

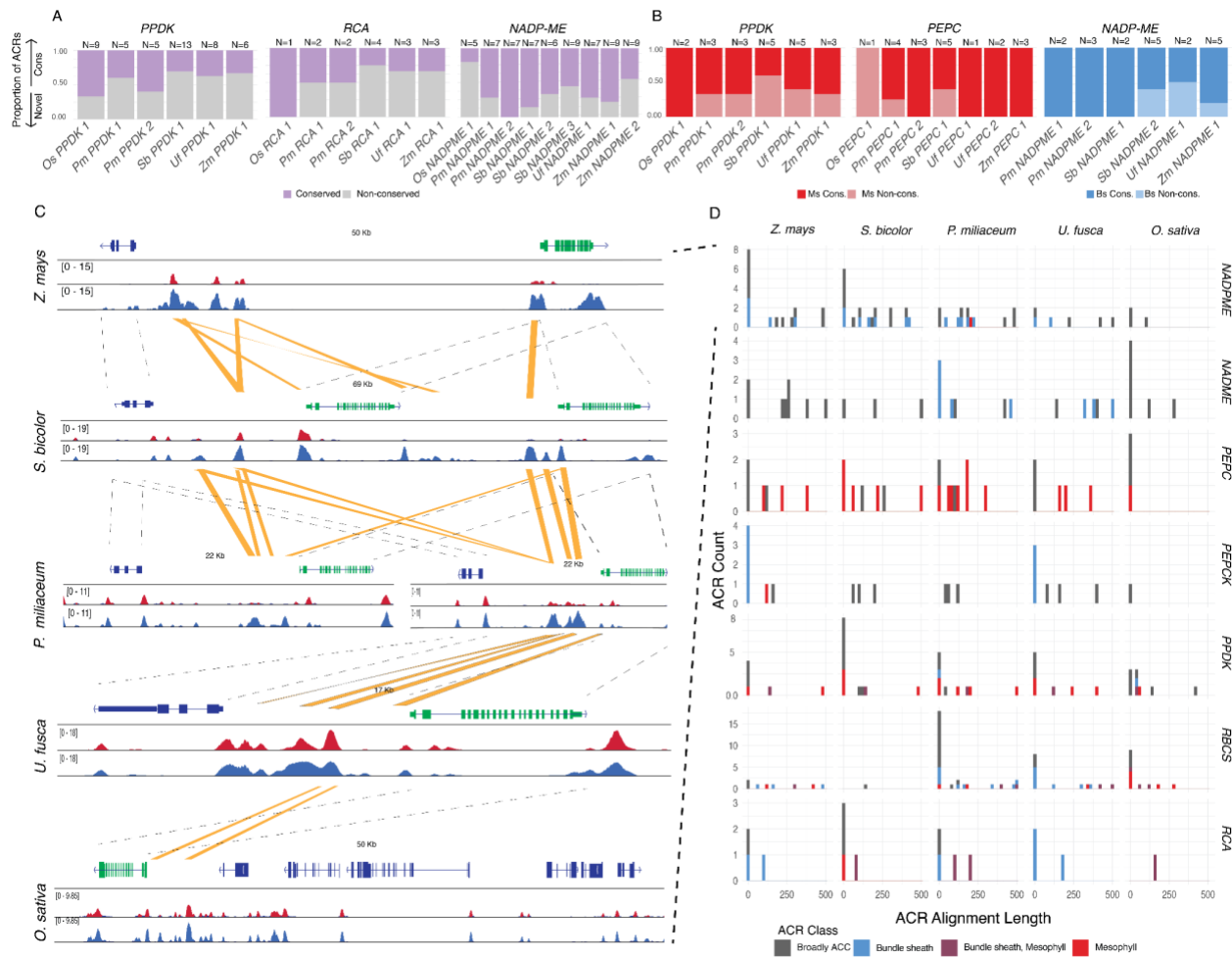
482 Although binary classification of ACRs was useful to decipher larger scale patterns  
483 between key enzymes, we next tested if larger segments of sequence were conserved around  
484 some  $C_4$  genes as compared to others. We profiled the relative amount of conserved sequence  
485 at each of these ACRs, as alignment of sequence between species gives greater resolution  
486 about important ACRs. One interesting observation from this analysis was the fact that the cell-  
487 type-specific ACRs around *PEPCK* appear to be novel between *Z. mays* and *U. fusca* (**Figure**  
488 **5D, Supplemental Figure 29-30**). This suggests that these regulatory loci emerged  
489 independently, and yet are still likely important in cell-type-specific expression of *PEPCK*.  
490 Additionally, around the *NAD-ME* loci in *P. miliaceum*, we found diverse evolutionary histories  
491 with both copies *NAD-ME1* and *NAD-ME2* having both conserved and novel BS-specific ACRs  
492 (one out of four ACRs were novel for *NAD-ME1*, and zero out of the two were conserved for  
493 *NAD-ME2*) (**Figure 5D**). The ACRs from *NADP-ME1* are conserved in *U. fusca*, whereas all  
494 three BS-specific ACRs are conserved in relation to *P. miliaceum*. Pointing to the fact that the  
495 ACRs have likely maintained their cell-type specificity, and are likely critical drivers in the correct  
496 expression of *NAD-ME* loci. These results highlight the dynamic evolution of cell-type-specific  
497 ACRs around key  $C_4$  loci, and that even closely related subtypes have evolved novel ACRs  
498 potentially critical in terms of proper gene expression, as well as compartmentalization.

499

500

501

502



503  
504

**Figure 5:** The evolutionary relationships of *cis*-regulatory regions around C4 genes is complex, being composed of both novel and conserved ACRs. **A)** The proportion of all ACRs that are conserved or novel for the following gene families *PPDK*, *RCA*, and *NADP-ME*. Purple bars represent ACRs that have any sequence aligned to them from a different species, and gray represents ACRs where sequences are not alignable. The number of ACRs in each locus is labeled at the top of each column. **B)** The proportion of cell-type-specific ACRs that are conserved and novel for the following gene families, *PPDK*, *PEPC*, and *NADP-ME*. Red bars only consider MS-specific ACRs, and blue bars only consider BS-specific ACRs. **C)** Screenshot of the conservation of BS-specific ACRs around *NADP-ME* across species. From top to bottom the species are *Z. mays*, *S. bicolor*, *P. miliaceum*, *U. fusca*, and *O. sativa*. *NADP-ME* is annotated in green for all species. Dashed bars between gene models represent the same gene model, and yellow bars are conserved ACRs. Browser tracks are blue for BS, and red for MS. Browser tracks are scaled within each species to allow for direct comparisons. **D)** The length of ACRs that are conserved in a cross species context. Rows represent gene families, and columns represent species. Each histogram is the number of ACRs within the loci of that gene family. The x-axis is the length of the ACR that is conserved and the y-axis is the count. ACRs are color coded according to the legend.

522

523

524 **Identification of *de novo* TF-Binding Motifs from Cell-type-specific Chromatin Data**  
525 **Reveals Rapid Sequence Diversification of ACRs**

526 Leveraging the cell-type-resolved datasets, we identified *de novo* cell-type-specific TF motifs in  
527 BS and MS ACRs (**Figure 6 A & B; Methods ; Supplemental Figure 31**). We selected the BS-  
528 specific motifs based on motif similarity within C<sub>4</sub> species for BS, and motif similarity seen  
529 across all species for MS. Additionally for the identification of BS specific motifs, we identified  
530 motifs which didn't appear to have a corresponding motif in *O. sativa* (**Methods**). Reassuringly,  
531 within the BS-specific motifs, we identified a DOF TF motif, which is a key driver in the switch to  
532 C<sub>4</sub> photosynthesis (29,53,54). In brief, the DOF TFs have been implicated as being potential  
533 drivers of proper gene expression in *Z. mays* C<sub>4</sub> genes, both as repressors and activators. For  
534 example, *ZmDOF30* has been implicated as being important in driving BS specific gene  
535 expression (29,53,54). In total we identified three BS-specific motifs, and four MS-specific *de*  
536 *novo* motifs that are shared between the species sampled (**Figure 6 A & B ; Supplemental**  
537 **Figure 31**). Using motif comparison tools, we were able to assign five out of the six motifs to  
538 a putative TF family, implicating potential novel regulators in BS-and MS-specific gene  
539 expression (**Methods ; Supplemental Figure 29**). We surveyed the C<sub>4</sub> ACRs for the presence  
540 and absence of these motifs to determine if they provide the information needed for cell-type  
541 specificity. We additionally overlaid our BLAST results from the previous analysis in order to  
542 explore the relationship between these motifs and conservation (**Figure 6C**). A substantial  
543 number of motifs were present within the non-conserved regions of the ACRs. For instance, in  
544 one MS-specific ACR associated with *ZmCA3.12/13* MS-specific motifs were found in non-  
545 conserved regions, suggesting these regions could be critical for driving the cell-type-specificity  
546 of this locus (**Figure 6D**).

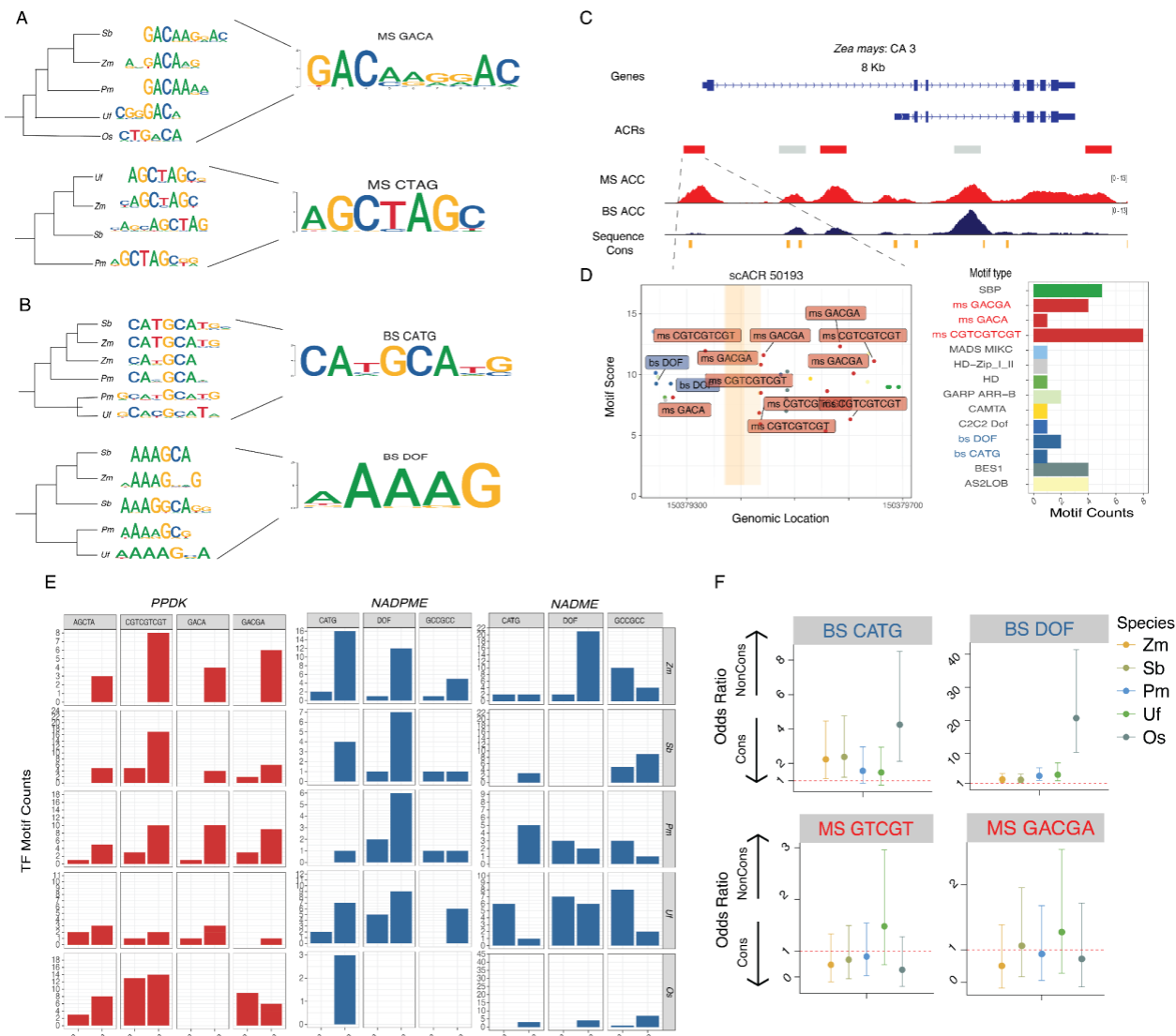
547 We expanded the analysis of BS- and MS-specific motifs in conserved and non-  
548 conserved regions of ACRs across key loci in the C<sub>4</sub> species. On average the MS-specific  
549 motifs are more conserved than the BS-specific motifs (**Figure 6E-F; Supplemental Figure 32**  
550). Agreeing with previous models of C<sub>4</sub> evolution where some motifs that are MS specific have  
551 been co-opted to operate in C<sub>4</sub> photosynthesis (**Figure 6D**) (11). Interestingly, we noticed a  
552 pattern where around *PPDK*, many of the MS-specific motifs appeared to be in non-conserved  
553 sequences for all of our species sampled (**Figure 6E**). This pattern is further highlighted in both  
554 *NADPME*, and *NADME* loci, where a majority of the BS-specific motifs occurred in non-  
555 conserved ACR regions for *NADPME*. This pattern is more nuanced in the *NADME* ACRs, as *P.*  
556 *miliaceum* and *U. fusca* share a significant amount of conserved sequence containing BS-  
557 specific motifs in the ACRs, suggesting that the BS-specific regulatory changes associated with  
558 these motifs are important (**Figure 6F**). These results highlight the capacity of genome-wide  
559 single-cell *cis*-regulatory maps to pinpoint key TF motifs important for the evolution of cell-type  
560 specificity.

561

562

563

564



565  
566  
567  
568  
569  
570  
571  
572  
573  
574  
575  
576  
577  
578  
579  
580

**Figure 6: Identification of cell-type-specific TF motifs reveal a complex relationship between sequence conservation and motif presence. A subsample of MS- (A) and BS-specific (B) de novo TF motifs identified. Left) De novo motifs were clustered by the correlation of their PWMs and a correlation based tree was generated. Right) Representative PWMs from de novo discovery. C) Screenshot of the *ZmCA3* locus. ACRs are color coded based on their cell-type specificity. MS- and BS-chromatin accessibility tracks are equally scaled for comparison. Sequence conservation is identified by the ACR having sequence homology to other CA ACRs from a different species. D) An example of the conservation and motif landscape of one MS-specific ACR at *ZmCA3*. Left, the location of the motifs in ACRs with MS- and BS-specific motifs labeled. Orange highlighted regions correspond to the region of sequence conservation seen above. Right, quantification of the motifs found in the ACR. X-axis is the motif count, and the y-axis is the motif. E) The counts of TF motifs in conserved and non-conserved ACRs for three different genes across all five species. Y-axis is the number of ACRs of a given type, and the x-axis indicates the type of ACR. F) Odds ratio of four motifs when comparing their enrichment in conserved versus non-conserved regions. A higher odds ratio indicates that the motif is more**

581 often found in non-conserved regions within ACRs, whereas a lower odds ratio means the motif  
582 is in conserved regions. The cell-type-specific motifs found in **A/B** are colored in red and blue,  
583 respectively.

584

### 585 **The DITs in the NADP-ME Subtypes Demonstrate Dynamic CRE Evolution**

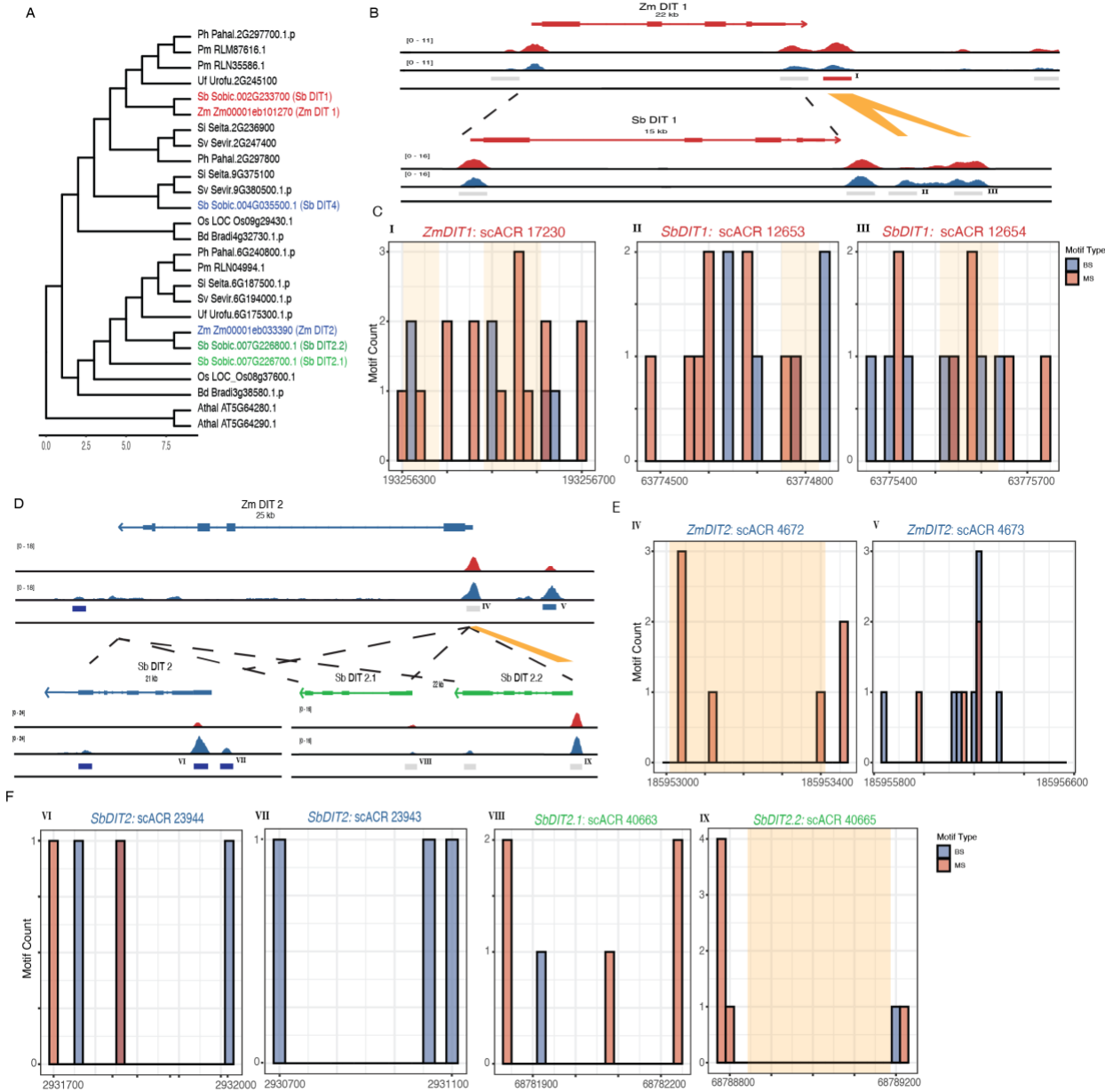
586 Upon analyzing the malate transporters *DICARBOXYLIC ACID TRANSPORTER*'s (*DITs*  
587 also known as the *DCTs*) we noticed the DITs in the NADP-ME subtypes showed an interesting  
588 pattern where the copies of *DIT1* in *Z. mays* and *S. bicolor* showed MS-specific chromatin  
589 accessibility, but the BS-specific copies of the *DITs* showed a more complex evolutionary  
590 history (**Figure 3B**; **Figure 7A**). We generated a phylogeny with additional species, and found  
591 that the BS-specific copy of *ZmDIT2* is related to two additional copies of *DITs* which are not  
592 BS-specific in *S. bicolor* (Here *SbDIT2.2* and *SbDIT2.1*) (**Figure 7A**). *S. bicolor* has a BS-  
593 specific copy of *SbDIT4*, which shares a clade with *ZmDIT1*. These results are consistent with  
594 earlier studies that found similar patterns and gene expression profiles of these copies of the  
595 *DITs* in *Z. mays* and *S. bicolor* (33,36,55). Although previous studies have documented changes  
596 in cell-type-specific gene expression for the BS-specific copies of the DITs, the mechanisms  
597 underlying these changes remain unclear. By using cell-type-specific ACRs, we explored if  
598 expression changes are associated with changes in the number of cell-type-specific cis-  
599 regulatory elements over evolutionary time.

600 To understand how cell-type specificity changed in these DITs due to changes in *cis*-  
601 regulation, we compared the ACRs associated with the *DITs*, and mapped the TF-binding motifs  
602 found within each ACR (**Methods**). For the MS-specific *DIT1*s, we focused on a MS-specific  
603 ACR located at the 3' end of *DIT1* in *Z. mays* (**Figure 7B**). Upon comparing this ACR to *S.*  
604 *bicolor*, we were struck that the sequence found in the *Z. mays* ACR was actually split in two in  
605 *S. bicolor*, neither of which demonstrated cell-type specificity in *S. bicolor* (**Figure 7B** ;  
606 **Supplemental Figure 33**). A closer inspection of motifs in these ACRs showed many MS-  
607 specific motifs (**Figure 7B-C**). These motifs might promote MS-specific gene expression of this  
608 locus. However, many *S. bicolor* MS-specific ACRs were not found in regions with any  
609 homology to *Z. mays* (**Figure 7C**). These results point to the rapid change of candidate CREs  
610 (cCREs) in this locus, and likely indicate that cCREs important in cell-type-specific gene  
611 expression might not be only found in conserved regulatory regions (56). Rather, selection of  
612 MS-specific gene expression is ongoing, and may yield significantly different regulatory  
613 environments in relatively short evolutionary time scales.

614 Next, we examined the BS-specific *ZmDIT2* and its two orthologs *SbDIT2.1* and  
615 *SbDIT2.2* , which are not BS specific (**Figure 7A, D**). The BS-specific ACR around *ZmDIT2* has  
616 many DOF TF motifs (**Figure 7E**). These motifs are interesting, as expression changes within  
617 the DOF TF family could be important in driving BS-specific gene expression in C<sub>4</sub> plants  
618 (29,53,57). When comparing the BS-specific ACRs around *ZmDIT4* to the more closely related  
619 copies of *SbDIT2.1* and *SbDIT2.2*, we found no conservation of these DOF TF motifs, and  
620 rather a significant lack of BS-specific TF motifs (**Figure 7F**). Considering the fact that neither of  
621 these *DIT* copies in *S. bicolor* show BS-specific expression, this result makes sense. Potentially  
622 providing a model where the *ZmDIT4* locus either gained these cCREs allowing for this copy of  
623 *ZmDIT2* to have BS specific gene expression, or *S. bicolor* lost these BS-specific motifs, and  
624 had a gain in *SbDIT4* specificity. In either scenario, it demonstrates the rapid pace of CRE

625 evolution, and how these regions might be altering cell-type-specific gene expression. These  
 626 results are in contrast to *SbDIT4*, where the ACRs around this locus are BS specific, and  
 627 contain BS-specific motifs identified in our previous analysis (**Figure 7F**). In total, these results  
 628 highlight the rapid rate of regulatory change around key C<sub>4</sub> loci, and highlight the fact that there  
 629 are likely key regulatory switches outside of conserved sequences. Finally, these results  
 630 emphasize the fast pace in which cell-type specificity changes in plants

631  
 632



633  
 634 **Figure 7: A)** Phylogenetic tree showing the evolutionary relationship of the *DITs* in the  
 635 monocots. *DITs* for *Z. mays* and *S. bicolor* are colored by their observed cell-type specificity,  
 636 with red being MS specific, and blue being BS specific. Additional species have been added to  
 637 increase resolution **B)** A screenshot of the *DIT1* between *Z. mays* (top) and *S. bicolor* (bottom).

638 Yellow boxes indicate ACR sequences with conserved homology **C/E/F**) Motif location of BS  
639 and MS specific motifs in each ACR. The x-axis is the location within the ACR, and the y-axis is  
640 the motif count. Yellow bars indicate regions of sequence homology. Within each histogram, the  
641 x-axis is binned into 20bp regions for ease of graphing. Roman numerals in the top corner  
642 highlight the corresponding ACR found in the screenshot. **(I-IX top)** X-axis the genomic  
643 coordinates of the given ACR. Yellow blocks denote the sequence homology as seen above. Y-  
644 axis, the motif score as calculated by motifmatchR, higher scores indicate a more confident  
645 motif. **bottom)** The count of each motif identified in the ACR. Note that BS and MS *de-novo*  
646 identified motifs are in blue and red respectively. **D)** A screenshot of the BS specific DITs loci  
647 between *Z. mays* (top) and *S. bicolor* (bottom). For the *S. bicolor* versions of the *DITs*, *DIT4* is  
648 colored blue for its observed BS specificity and *DIT2.1* and *DIT2.2* are colored green. Yellow  
649 boxes indicate sequence homology.

650  
651

## 652 Discussion:

653 Understanding the evolution of *cis*-regulation associated with C<sub>4</sub> photosynthesis has  
654 been a long standing goal in the field of plant biology. In this study, we demonstrated the utility  
655 of single-cell ATAC-seq data to investigate many aspects of the evolution of C<sub>4</sub> photosynthesis.  
656 By identifying cell-type-specific chromatin accessibility from four C<sub>4</sub> species composed of three  
657 different C<sub>4</sub> subtypes, as well as a single C<sub>3</sub> outgroup, we were able to compare and contrast  
658 key genes and their ACRs which define and distinguish C<sub>4</sub> photosynthesis. We have shown that  
659 by using gene-body chromatin accessibility data, we can measure cell-type-specific bias of both  
660 core, and subtype-specific C<sub>4</sub> enzymes. When taken into consideration with the gene family  
661 trees of many of these enzymes, we show diverse co-option of enzymes into the C<sub>4</sub> pathway.  
662 Additionally, we identify cell-type-specific ACRs surrounding these key C<sub>4</sub> enzymes. We find  
663 numerous cell-type-specific ACRs surrounding key C<sub>4</sub> enzymes, many of which fall outside of  
664 the core promoter region. Additionally we find that around all of the C<sub>4</sub> enzymes there is a mix of  
665 both conserved and novel cell-type-specific ACRs indicating that regulatory evolution of these  
666 regions is ongoing. Finally, we use cell-type-specific ACRs to identify a series of *de-novo*  
667 binding motifs which appear to be cell-type specific, and show that these motifs surround C<sub>4</sub>  
668 loci, and have a mixed relationship with conservation depending on the motif. This indicates that  
669 cell-type-specific TF motifs are rapidly changing around C<sub>4</sub> loci.

670 Investigation of the CREs driving cell-type-specific expression of C<sub>4</sub> genes is  
671 challenging. This often requires evaluation using transgenic plants, which limits the number of  
672 CREs that can be tested. This has greatly hampered efforts at understanding how *cis*-regulation  
673 of C<sub>4</sub> genes evolves, whether by co-option of existing CREs or emergence of new ones. Our  
674 results show the complex nature of CRE evolution of C<sub>4</sub> genes, including those specific to C<sub>4</sub>  
675 subtypes. While we observe conservation of ACRs around many C<sub>4</sub> genes, we do see  
676 interesting examples where the subtype-specific enzymes have evolved novel ACRs (*NAD-*  
677 *ME*'s in *P. miliaceum*, and *PEPCK* in *U. fusca*). These results support that there is likely a  
678 combination of both co-opting pre-existing CREs, as well as evolving new ones to facilitate  
679 proper expression and cell-type-specification of genes. This is further exemplified by the  
680 analysis of the *DIT* family of transporters, where we show striking accumulation of cell-type-

681 specific TF motifs in non-conserved regions of ACRs between two closely related species. This  
682 highlights that the regions of the genome promoting cell-type-specific gene expression are likely  
683 found in both conserved, and novel regions. Another recent single-cell genomic study of the  
684 evolution of CREs important for photosynthesis using a comparison between *O. sativa* and *S.*  
685 *bicolor* reached similar conclusions (57). They frequently found different ACRs and TF motifs in  
686 promoters of orthologous C<sub>4</sub> genes (57). Future efforts to assay these candidate CREs using  
687 reporter assays, transgenesis and genome editing will be required. Additionally, expanding  
688 these analysis outward to all genes associated with photosynthesis might provide valuable  
689 insights into how genes in the Calvin-Benson cycle alter their regulation in their adaptation to C<sub>4</sub>  
690 photosynthesis. Fortunately, these high-resolution maps of cell-type-specific ACRs of these key  
691 genes/species provide a strong foundation to build upon.

692 Although these studies provide a blueprint for the study of key candidate CREs  
693 associated with C<sub>4</sub> enzymes, profiling cell-type-specific chromatin accessibility of additional  
694 species would be greatly beneficial. Although *O. sativa* is an invaluable outgroup for this study,  
695 additional more closely related C<sub>3</sub> species might make these comparisons simpler, and add  
696 additional resolution. For instance the C<sub>3</sub> grass species *Dichanthelium oligosanthes* is more  
697 closely related to *U. fusca* and *P. miliaceum* and has a recently completed reference genome  
698 (58). Adding more species would enable greater resolution in the comparison of cell-type-  
699 specific ACRs, as the genetic distance between the species we examined and *O. sativa* make  
700 identification of conserved and novel ACRs challenging. As an example, the ACRs associated  
701 with NAD-ME's in *P. miliaceum* might be co-opted instead of novel, however, based on our  
702 sampling, we cannot say.

703 Genome editing analysis of many of these ACRs would significantly advance which  
704 ACRs, and more specifically which CREs within the ACRs are most important for cell-type-  
705 specific expression (22). However, currently generating genome edits in monocots is  
706 challenging, time consuming and expensive. Fortunately, improvements to transgenesis are  
707 constantly improving making achieving these goals more likely in the future (59). It's also  
708 important to consider that mutational analysis of CREs is not straightforward, often requiring  
709 numerous editing events of the *cis*-regulatory landscape of each gene. Previous studies have  
710 shown that deletions of many CREs produce variable molecular and morphological phenotypes,  
711 further complicating our understanding of the *cis*-regulatory code (60–62). And finally, many  
712 species, including *P. miliaceum* and *U. fusca* have to date never been transformed. This  
713 highlights the need to continually improve transgenesis methods to help facilitate the molecular  
714 dissection of CRE. In conclusion, this study provides a comprehensive map of cell-type-specific  
715 ACRs around key C<sub>4</sub> genes, which reveals the dynamic evolution and diversity of *cis*-regulation  
716 of C<sub>4</sub> genes.

717  
718

## 719 **Acknowledgments:**

720 This research was funded by awards from the National Science Foundation (IOS-2134912 and  
721 IOS-1856627) and the Office of Research to RJS and Hong Kong University Grant Council  
722 (GRF 1409420) to SZ. APM and JPM were supported by the National Institutes of Health  
723 (K99GM144742) and (T32GM142623), respectively. This research was additionally funded with

724 support from the NSFC (32100438 & 32370247) and Shanghai Jiao Tong University 2030  
725 Initiative (to X.T.).  
726

## 727 **Methods:**

### 728 **Plant Growth Conditions and Sampling:**

729 Seedlings of all five plant species, including maize (*Zea mays* B73), sorghum (*Sorghum bicolor*  
730 BTx623), proso millet (*Panicum miliaceum* L. CGRIS 00000390), and browntop signalgrass  
731 (*Urochloa fusca* LBJWC-52), along with the C<sub>3</sub> plant rice (*Oryza sativa* Nipponbare), were grown  
732 under the conditions of 12:12 Light/Dark cycles at 30°C Light/22°C Dark and at 50% humidity.  
733 The sampling of the C<sub>4</sub> species was timed to coincide with a specific developmental stage,  
734 identified when the ligule of the third leaf became visible, marking the third leaf unfolding, yet  
735 prior to the appearance of the fourth leaf. For the C<sub>3</sub> species, rice, 18-day-old leaves were used  
736 to correspond with the equivalent stage of the C<sub>4</sub> species.  
737

### 738 **Library Preparation:**

739 Nuclei isolation for the experiments was conducted using fresh seedlings of both the C<sub>4</sub> and C<sub>3</sub>  
740 species at their respective developmental stages. The methodology for nuclei extraction,  
741 encompassing the buffer composition and the subsequent steps, was used with procedures  
742 outlined for single-nucleus combinatorial indexing with transposed-based ATAC-seq library  
743 construction, as detailed in a prior study (63).  
744

### 745 **Genomes:**

746 The *Z. mays* genome version 5 was downloaded from MaizeGDB (64,65). The *O. sativa*  
747 genome was downloaded from rice.uga.edu. The *S. bicolor* version v5.1 was downloaded and  
748 used from Phytozome version 13, as well as the *U. fusca* genome version 1.1 (66). Finally the  
749 *P. miliaceum* genome was downloaded from NCBI, bioproject number PRJNA431363 (43).  
750

### 751 **Barcode Correction Read Alignment and Mapping of Tn5 Insertions:**

752 Read UMIs were processed using cutadapt (version 4.5) to identify UMIs (67). First, the index  
753 adapter sequences were trimmed from the reads. Next, the well barcodes and Tn5 barcode  
754 within the reads were identified, removed from the original sequencing read, and appended to  
755 the read header. Finally, a shell script is used to integrate all barcode information from the  
756 reads' headers and label them correspondingly in the paired-end sequencing fastq files. Reads  
757 were aligned using BWA (version 0.7.17) (68). Reads were filtered using samtools (version  
758 1.16.1) for mapping quality of >10 for *Z. mays*, *S. bicolor*, *U. fusca*, and *O. sativa*. *P. miliaceum*  
759 required a greater threshold of 30 given its recent whole genome duplication event increasing  
760 the rate of multi-mapping reads (69). Duplicate reads were removed using picard tools (version  
761 2.25.0) (70). Single-base pair Tn5 integration events were mapped using the python script  
762 `makeTn5bed.py` found in the GitHub utils directory  
763 ([https://github.com/Jome0169/Mendieta.C4\\_manuscript](https://github.com/Jome0169/Mendieta.C4_manuscript)). Finally, for each barcode only unique  
764 Tn5 integrations sites were used for analysis. So if a nuclei had the same identical fragments  
765 multiple times, only a single event was considered.  
766

767 **Isolating High-Quality Cells:**

768 Cells were filtered using Socrates (21). In short, Fraction of Reads in Peaks (FRiP) scores were  
769 calculated for each cell by pseudo bulking the libraries and identifying peaks. For each  
770 individual cell, FRiP was calculated by intersecting Tn5 integration events with peaks. Cells with  
771 a FRiP score greater than 0.2 were used. Additionally, TSS enrichment was calculated by  
772 looking at the number of Tn5 integrations around TSS. Cells that had a TSS enrichment greater  
773 than 0.15 were used. Finally, cells were compared to a random sample of low quality cells which  
774 did not pass filtering, representing the “background” of cells, and correlation was calculated  
775 between passing cells and background cells using the corr package in R. Cells which had a  
776 correlation lower than 0.3 percent as compared to background cells were used for further  
777 analysis.

778 UMAP embeddings were then calculated for each species utilizing genomic bins (71).  
779 For each dataset, bins of 500 bp were calculated. To reduce the size of features to cluster on,  
780 bins had to show accessible chromatin in at least 0.005% of total cells (roughly 50~100 cells in  
781 each species). Additionally, bins that were broadly accessible across greater than 10% of cells  
782 in the given dataset were also discarded to remove regions of the genome which were  
783 constitutively accessible and wouldn't facilitate clustering. Finally, regions of the genome which  
784 were associated with either blacklist (21), or genes which were known to be related to cell cycle  
785 and circadian rhythms were removed. The final resulting matrix, which represented cell  
786 barcodes X genomic regions (here bins), were then put through the term-frequency inverse-  
787 document-frequency (TF-IDF) algorithm to identify genomic regions more descriptive of the  
788 entire dataset (30). The resulting matrix was then input into Singular Value Decomposition, and  
789 clustering was then done on the remaining features with the number of principal components  
790 (PCs) equaling 50, and any PC with a correlation to read depth greater than 0.5 removed (72)  
791 (30). Clustering was done using the Louvain clustering algorithm in order to bin cells into similar  
792 groups based off of the PCs calculated above, with parameters “res = 1.5, k.near = 30, m.dist =  
793 .01” in order to set K nearest neighbors to 30, minimum louvain distance to .01 in euclidean  
794 space (73). Using the UMAP embeddings, doublets were removed using the software Scrublet  
795 as implemented in Socrates software (74). At random, 5,000 cells were used to generate *in-*  
796 *silico* doublets, and cells which were scored as being likely doublets were removed. Adaptive  
797 thresholds were set on a per library basis. The doublet rate from Scrublet was compared  
798 against a mixed library where genotypes of *Z. mays* were mixed Mo17 and B73, and genotype  
799 doublets were identified. We found that Scrublet, on average, removed more cells in a  
800 conservative fashion than the birthday problem and genotype doublets identified, so we utilized  
801 the Scrublet doublet scores to be conservative. For the *P. miliaceum* dataset, replicates were  
802 found to integrate poorly in the UMAP embedding. Harmony (version 0.1.1) was used to adjust  
803 replicate overlap with parameters “theta = 2, nclust=4, and var = “sampleID” (75). After  
804 integration, clusters which skewed greater than 75% towards one replicate were removed from  
805 downstream analysis.

806

807 **Identification of Putative Orthologs:**

808 To annotate species with less marker gene information, we identified putative orthologs or  
809 marker genes using OrthoFinder (version 2.5.4) (31). For each species, the primary protein  
810 sequence of the transcript was used as input to Orthofinder. In the resulting orthofinder outputs,

811 the script “find\_markers.orthofinder.py” was used to parse the resulting phylogenies and return  
812 back putative orthologs ([https://github.com/Jome0169/Mendieta.C4\\_manuscript](https://github.com/Jome0169/Mendieta.C4_manuscript)). For all C<sub>4</sub>  
813 genes analyzed, each orthogroup was additionally annotated by hand in order to ensure  
814 accurate assignment of nearest orthologs phylogenetically.  
815

#### 816 **Annotation of Cell Types:**

817 Cell types were annotated by calculating gene chromatin accessibility for marker genes in each  
818 genome on a per cell basis. These values were then visualized on the UMAP embedding, and  
819 clusters with numerous marker genes associated with the same cell-type were used as  
820 evidence. Additionally, for each louvain cluster, enrichment of marker genes was calculated by  
821 comparing the cluster average as compared to a random shuffle of random cells. The top five  
822 most enriched markers were used in tandem with the UMAPs to ascertain cell-type identity. We  
823 also tested the statistical significance of the marker gene using Presto, a modified Wilcoxon  
824 rank-sum test in order to identify the most unique marker gene in each cluster (76). Additionally,  
825 for specific clusters showing mixed signals from marker genes, sub-clustering was done by  
826 isolating the cluster in question, and then re-clustering these cells on a new UMAP manifold.  
827 The same steps were done to visualize marker genes, as well as test this enrichment, and  
828 statistical significance. Finally, to bolster our set of marker genes across species, we used our  
829 most confident cell-type annotation in *Z. mays* to *de novo* discover marker genes. To do so, we  
830 utilized our gene-body-accessibility metrics for each annotated cell-type, and ran DESeq2  
831 (version 1.42.0) in a replicate aware fashion using all other cells as a null (77). Only statistically  
832 significant markers were kept which had a fold change greater than 1.5, and a log fold standard  
833 error of less than .6. OrthoFinder was used as mentioned above to find orthologs. To ensure  
834 that we were comparing similar cell-types, we also took an orthogonal approach where we  
835 compared the gene accessibility of the top 2000 most variable orthologs between our species. A  
836 linear model was used for each species comparison where the mean gene accessibility was  
837 taken into consideration, and the species was one-hot-encoded. Variation was calculated as the  
838 average variation between both datasets. The resulting residuals were used to generate the  
839 cell-type correlations.  
840

#### 841 **Peak Identification:**

842 To identify peaks, cells of the same annotation type were pseudo bulked in a replicate aware  
843 fashion. Within each replicate MACS2 (version 2.2.9.1) was run with parameters “--nomodel --  
844 keep-dup auto --extsize 150 --shift -75 --qvalue .05” and variable genome size flag ‘-g’ (78).  
845 Summits for each peak identified in each replicate were extended by 250 bp in either direction.  
846 Only peaks which overlapped between replicates were used. To merge peaks from various cell  
847 types and select peak boundaries, the p-value associated with each peak in each cell type was  
848 compared by calculating the chromatin accessibility score for each peak per million, with those  
849 peaks with the highest accessibility score being selected as the representative peak. This  
850 method of identifying the most representative peaks across cell-types was inspired by previous  
851 single cell ATAC-seq papers (30,79,80). Additionally, bigwigs were generated for each cell type  
852 by normalizing each dataset to the number of reads/per million scaling factor. Implementation of  
853 this algorithm is found in the script call\_scACRs.py for ease of use and replication in other  
854 experiments.

855

### 856 **Identifying Cell-type-specific ACRs:**

857 To identify cell-type specific ACRs, a modified bootstrapping method was used which drew  
858 inspiration from the modified entropy metrics found in (79). On a per ACR basis, Tn5  
859 integrations per cell-type were summed and counts per million (CPM) normalized. These values  
860 were then converted to a probability by using the following equation (below, equation 1) where  
861  $pi$  is the CPM value for the focal cell-type and  $qi$  is the total sum of all CPMs. From this  
862 probability statement, a modified shannon entropy metric was calculated, followed by a metric of  
863 specificity  $Qpt$ . For robust cell-type-specific ACR identification, the annotated cell-type was  
864 bootstrapped 5000 times, taking a sample of 250 cells from the cell population in question, and  
865 calculating both entropy and specificity scores. This was done to attempt to get a robust signal  
866 of specificity, which takes into consideration the variation in cell quality present in each cell-type  
867 annotation. To generate the null distribution of specificity scores, individual cell annotations  
868 were scrambled to generate an equal number of null cell-type classifications. For each null  
869 value, the entropy and specificity score were calculated. Finally to calculate a p-value, a non-  
870 parametric approach was used to identify how many of the real bootstraps fell outside of the null  
871 distribution using a one tailed test. ACRs which had a p-value of  $<0.001$  were considered to be  
872 significant. ACRs were finally classified by the number of cell types they were specific to. ACRs  
873 specific to greater than three were classified as broadly accessible, less than or equal to three  
874 as cell type restricted, and a single cell-type as cell-type specific.

875 1)  $pi = \frac{qi}{\Sigma(qi)}$

876 2)  $Hp = -\sum pi \log_2(pi)$

877 3)  $Qpt = Hp - \log_2(Hp)$

878

### 879 **Identifying Conserved ACRs Across Species**

880 Since a majority of the C4 genes identified were not in synteny with one another, we took a  
881 gene family based approach to identify conserved and non-conserved ACRs associated with  
882 our C4 genes. In short, all ACRs within two gene models of a C4 gene are utilized for  
883 comparison. Sequences from the ACR were isolated using “bedtools getfasta” (version 2.31)  
884 (81). Then in a pairwise fashion each species had their ACRs from one C4 gene family  
885 compared to the corresponding genomic loci of the same gene family in a different species.  
886 Comparisons were made using Blastn (version 2.2.29) with the following parameters “ -task  
887 blastn-short -evalue 1e-3 -max\_target\_seqs 4 -word\_size 7 -gapopen 5 -gapextend 2 -penalty -1  
888 -reward 1 -dust no -outfmt 6 ” (82). The output blast files were further filtered requiring sequence  
889 alignment to be greater than 20 nts, and have an evalue of .001. This analysis and the detailed  
890 commands ran can be found in the following snakemake file titled  
891 “ID\_syntenic\_orthologous.ACRs.snake”, and found in the snakemake directory in the associated  
892 github.

893

### 894 **Identifying Cell-type-specific Motifs:**

895 *De-novo* cell-type-specific motifs were identified by using XSTREME (version 5.5.3) of the  
896 MEME suite (version 5.5.5) package (83,84). In brief the sequences underlying the cell-type-  
897 specific ACRs were isolated, and equally matched null set of broadly-accessible ACRs were  
898 used the comparison for genomic enrichment. These null ACRs were matched in terms of GC

899 content, and were only allowed to be 5% different from the cell-type-specific set in question and  
900 generated using the script “gen\_null\_fa.py”. Upon generation, motifs were analyzed using the  
901 universalmotifs package in R (version 3.18) (85). Motifs were first compared using HELL  
902 distance, and motifs which had a low correlation were discarded. In order to generate  
903 representative motifs, highly correlated motifs were merged using the function “merge\_motifs” in  
904 found in the universalmotifs package. To identify the location of motifs, the R package  
905 motifmatchR were used, with a significant value cut off of .0005 (86).  
906

#### 907 **Motifs Comparison:**

908 In order to compare *de novo* identified motifs, position weight matrices were compared to using  
909 TomTom (version 5.5.5). Motifs were compared either against the non-redundant TF database  
910 for JASPAR plant TF binding motifs, or compared versus the consensus sequences found in  
911 Zenker et al 2024. The most significant motif was used to assign to potential TF families (87–  
912 89).  
913

#### 914 **Data availability:**

915 sciATAC-seq data for *Z. mays*, *S. bicolor*, *U. fusca*, and *P. miliceum* is found in NCBI under the  
916 following bioproject PRJNA1063172. Leaf data for *O. sativa* can be found under the following  
917 SRR bioproject PRJNA100757. All scripts used for processing and analyzing data in this  
918 manuscript can be found at the following github repository:

919 [https://github.com/Jome0169/Mendieta.C4\\_manuscript](https://github.com/Jome0169/Mendieta.C4_manuscript) . Additionally, all datasets with both MS  
920 and BS specific accessibility profiles, their ACRs, as well as their BLASTN relationships can be  
921 found on the epigenome browser <https://epigenome.genetics.uga.edu/PlantEpigenome>. All  
922 datasets can be found under the sub-folder Mendieta\_et\_al.C4\_project.  
923  
924

## 925 **References:**

- 926 1. Bowes G, Ogren WL, Hageman RH. Phosphoglycolate production catalyzed by ribulose  
927 diphosphate carboxylase. *Biochem Biophys Res Commun*. 1971 Nov 5;45(3):716–22.
- 928 2. Wheeler T, von Braun J. Climate Change Impacts on Global Food Security. *Science*. 2013  
929 Aug 2;341(6145):508–13.
- 930 3. Hatch MD. C4 photosynthesis: a unique blend of modified biochemistry, anatomy and  
931 ultrastructure. *Biochim Biophys Acta BBA - Rev Bioenerg*. 1987 Jan 1;895(2):81–106.
- 932 4. Offermann S, Okita TW, Edwards GE. Resolving the Compartmentation and Function of C4  
933 Photosynthesis in the Single-Cell C4 Species *Bienertia sinuspersici*. *Plant Physiol*. 2011 Apr  
934 1;155(4):1612–28.
- 935 5. Akhani H, Barroca J, Koteeva N, Voznesenskaya E, Franceschi V, Edwards G, et al.  
936 *Bienertia sinuspersici* (Chenopodiaceae): A New Species from Southwest Asia and  
937 Discovery of a Third Terrestrial C4 Plant Without Kranz Anatomy. *Syst Bot*. 2005 Apr  
938 1;30(2):290–301.
- 939 6. Sage RF. A portrait of the C<sub>4</sub> photosynthetic family on the 50th anniversary of its discovery:  
940 species number, evolutionary lineages, and Hall of Fame. *J Exp Bot*. 2016 Jul;67(14):4039–  
941 56.
- 942 7. Sage RF, Christin PA, Edwards EJ. The C4 plant lineages of planet Earth. *J Exp Bot*. 2011  
943 May 1;62(9):3155–69.

944 8. Gowik U, Westhoff P. The Path from C3 to C4 Photosynthesis. *Plant Physiol.* 2011 Jan  
945 1;155(1):56–63.

946 9. Grass Phylogeny Working Group II. New grass phylogeny resolves deep evolutionary  
947 relationships and discovers C4 origins. *New Phytol.* 2012 Jan;193(2):304–12.

948 10. Rao X, Dixon RA. The Differences between NAD-ME and NADP-ME Subtypes of C4  
949 Photosynthesis: More than Decarboxylating Enzymes. *Front Plant Sci [Internet].* 2016 [cited  
950 2023 May 22];7. Available from: <https://www.frontiersin.org/articles/10.3389/fpls.2016.01525>

951 11. Kajala K, Brown NJ, Williams BP, Borrill P, Taylor LE, Hibberd JM. Multiple *Arabidopsis*  
952 genes primed for recruitment into C4 photosynthesis. *Plant J.* 2012;69(1):47–56.

953 12. Sheen J. C4 Gene Expression. *Annu Rev Plant Physiol Plant Mol Biol.* 1999;50(1):187–217.

954 13. Chollet R, Vidal J, O’Leary MH. PHOSPHO ENOL PYRUVATE CARBOXYLASE: A  
955 Ubiquitous, Highly Regulated Enzyme in Plants. *Annu Rev Plant Physiol Plant Mol Biol.*  
956 1996 Jun;47(1):273–98.

957 14. O’Leary MH. Phosphoenolpyruvate Carboxylase: An Enzymologist’s View. *Annu Rev Plant  
958 Physiol.* 1982 Jun;33(1):297–315.

959 15. Outlaw Jr William H. Kinetic Properties of Guard-Cell Phosphoenolpyruvate Carboxylase.  
960 *Biochem Physiol Pflanz.* 1990 Jan 1;186(5):317–25.

961 16. Matsuoka M, Numazawa T. CIS-acting elements in the pyruvate, orthophosphate dikinase  
962 gene from maize. *Mol Gen Genet MGG.* 1991 Aug 1;228(1):143–52.

963 17. Ku MS, Agarie S, Nomura M, Fukayama H, Tsuchida H, Ono K, et al. High-level expression  
964 of maize phosphoenolpyruvate carboxylase in transgenic rice plants. *Nat Biotechnol.* 1999  
965 Jan;17(1):76–80.

966 18. Nomura M, Sentoku N, Nishimura A, Lin JH, Honda C, Taniguchi M, et al. The evolution of  
967 C4 plants: acquisition of cis-regulatory sequences in the promoter of C4-type pyruvate,  
968 orthophosphate dikinase gene. *Plant J.* 2000;22(3):211–21.

969 19. Gowik U, Burscheidt J, Akyildiz M, Schlué U, Koczor M, Streubel M, et al. cis-Regulatory  
970 Elements for Mesophyll-Specific Gene Expression in the C4 Plant *Flaveria trinervia*, the  
971 Promoter of the C4 Phosphoenolpyruvate Carboxylase Gene[W]. *Plant Cell.* 2004 May  
972 12;16(5):1077–90.

973 20. Kim ED, Dorrity MW, Fitzgerald BA, Seo H, Sepuru KM, Queitsch C, et al. Dynamic  
974 chromatin accessibility deploys heterotypic cis/trans-acting factors driving stomatal cell-fate  
975 commitment. *Nat Plants.* 2022 Dec;8(12):1453–66.

976 21. Marand AP, Chen Z, Gallavotti A, Schmitz RJ. A cis-regulatory atlas in maize at single-cell  
977 resolution. *Cell.* 2021 May 27;184(11):3041–3055.e21.

978 22. Meng F, Zhao H, Zhu B, Zhang T, Yang M, Li Y, et al. Genomic editing of intronic enhancers  
979 unveils their role in fine-tuning tissue-specific gene expression in *Arabidopsis thaliana*. *Plant  
980 Cell.* 2021 Mar 25;33(6):1997–2014.

981 23. Spitz F, Furlong EEM. Transcription factors: from enhancer binding to developmental  
982 control. *Nat Rev Genet.* 2012 Sep;13(9):613–26.

983 24. Matsuoka M, Kyozuka J, Shimamoto K, Kano-Murakami Y. The promoters of two  
984 carboxylases in a C4 plant (maize) direct cell-specific, light-regulated expression in a C3  
985 plant (rice). *Plant J.* 1994;6(3):311–9.

986 25. Matsuoka M, Tada Y, Fujimura T, Kano-Murakami Y. Tissue-specific light-regulated  
987 expression directed by the promoter of a C4 gene, maize pyruvate,orthophosphate dikinase,  
988 in a C3 plant, rice. *Proc Natl Acad Sci.* 1993 Oct 15;90(20):9586–90.

989 26. Gowik U, Schulze S, Saladié M, Rolland V, Tanz SK, Westhoff P, et al. A MEM1-like motif  
990 directs mesophyll cell-specific expression of the gene encoding the C4 carbonic anhydrase  
991 in *Flaveria*. *J Exp Bot.* 2017 Jan 1;68(2):311.

992 27. Gupta SD, Levey M, Schulze S, Karki S, Emmerling J, Streubel M, et al. The C4Ppc  
993 promoters of many C4 grass species share a common regulatory mechanism for gene  
994 expression in the mesophyll cell. *Plant J.* 2020;101(1):204–16.

995 28. Tu X, Ren S, Shen W, Li J, Li Y, Li C, et al. Limited conservation in cross-species  
996 comparison of GLK transcription factor binding suggested wide-spread cistrome divergence.  
997 *Nat Commun.* 2022 Dec 9;13(1):7632.

998 29. Dai X, Tu X, Du B, Dong P, Sun S, Wang X, et al. Chromatin and regulatory differentiation  
999 between bundle sheath and mesophyll cells in maize. *Plant J* [Internet]. 2022 Jan 14 [cited  
1000 2022 Jan 14];n/a(n/a). Available from:  
1001 <https://onlinelibrary.wiley.com/doi/abs/10.1111/tpj.15586>

1002 30. Cusanovich DA, Hill AJ, Aghamirzaie D, Daza RM, Pliner HA, Berletch JB, et al. A Single-  
1003 Cell Atlas of In Vivo Mammalian Chromatin Accessibility. *Cell*. 2018 Aug;174(5):1309-  
1004 1324.e18.

1005 31. Emms DM, Kelly S. OrthoFinder: phylogenetic orthology inference for comparative  
1006 genomics. *Genome Biol.* 2019 Nov 14;20(1):238.

1007 32. Taniguchi M, Sugiyama T. The Expression of 2-Oxoglutarate/Malate Translocator in the  
1008 Bundle-Sheath Mitochondria of *Panicum miliaceum*, a NAD-Malic Enzyme-Type C4 Plant, Is  
1009 Regulated by Light and Development. *Plant Physiol.* 1997 May 1;114(1):285-93.

1010 33. Taniguchi Y, Nagasaki J, Kawasaki M, Miyake H, Sugiyama T, Taniguchi M. Differentiation  
1011 of Dicarboxylate Transporters in Mesophyll and Bundle Sheath Chloroplasts of Maize. *Plant*  
1012 *Cell Physiol.* 2004 Feb 15;45(2):187-200.

1013 34. Tausta SL, Li P, Si Y, Gandotra N, Liu P, Sun Q, et al. Developmental dynamics of Kranz  
1014 cell transcriptional specificity in maize leaf reveals early onset of C4-related processes. *J*  
1015 *Exp Bot.* 2014 Jul;65(13):3543-55.

1016 35. Borba AR, Reyna-Llorens I, Dickinson PJ, Steed G, Gouveia P, Górska AM, et al.  
1017 Compartmentation of photosynthesis gene expression in C4 maize depends on time of day.  
1018 *Plant Physiol.* 2023 Aug 9;kiad447.

1019 36. Weissmann S, Huang P, Wiechert MA, Furuyama K, Brutnell TP, Taniguchi M, et al.  
1020 DCT4—A New Member of the Dicarboxylate Transporter Family in C4 Grasses. *Genome*  
1021 *Biol Evol.* 2021 Feb 1;13(2):eva251.

1022 37. Nomura M, Higuchi T, Katayama K, Taniguchi M, Miyao-Tokutomi M, Matsuoka M, et al.  
1023 The Promoter for C4-type Mitochondrial Aspartate Aminotransferase Does not Direct Bundle  
1024 Sheath-specific Expression in Transgenic Rice Plants. *Plant Cell Physiol.* 2005 May  
1025 1;46(5):743-53.

1026 38. Taniguchi M, Kobe A, Kato M, Sugiyama T. Aspartate Aminotransferase Isozymes in  
1027 *Panicum miliaceum* L, an NAD-Malic Enzyme-Type C4 Plant: Comparison of Enzymatic-  
1028 Properties, Primary Structures, and Expression Patterns. *Arch Biochem Biophys.* 1995 Apr  
1029 20;318(2):295-306.

1030 39. Taniguchi M, Sawaki H, Sasakawa H, Hase T, Sugiyama T. Cloning and sequence analysis  
1031 of cDNA encoding aspartate aminotransferase isozymes from *Panicum miliaceum* L., a C4  
1032 plant. *Eur J Biochem.* 1992;204(2):611-20.

1033 40. Son D, Jo J, Sugiyama T. Purification and characterization of alanine aminotransferase from  
1034 *Panicum miliaceum* leaves. *Arch Biochem Biophys.* 1991 Aug 15;289(1):262-6.

1035 41. Furumoto T, Yamaguchi T, Ohshima-Ichie Y, Nakamura M, Tsuchida-Iwata Y, Shimamura  
1036 M, et al. A plastidial sodium-dependent pyruvate transporter. *Nature.* 2011  
1037 Aug;476(7361):472-5.

1038 42. Wang Y, Bräutigam A, Weber APM, Zhu XG. Three distinct biochemical subtypes of C4  
1039 photosynthesis? A modelling analysis. *J Exp Bot.* 2014 Jul 1;65(13):3567-78.

1040 43. Zou C, Li L, Miki D, Li D, Tang Q, Xiao L, et al. The genome of broomcorn millet. *Nat*  
1041 *Commun.* 2019 Jan 25;10(1):436.

1042 44. Washburn JD, Strable J, Dickinson P, Kothapalli SS, Brose JM, Covshoff S, et al. Distinct  
1043 C4 sub-types and C3 bundle sheath isolation in the Paniceae grasses. *Plant Direct.*  
1044 2021;5(12):e373.

1045 45. Engineer C, Hashimoto-Sugimoto M, Negi J, Israelsson-Nordstrom M, Azoulay-Shemer T,

1046 Rappel WJ, et al. CO<sub>2</sub> sensing and CO<sub>2</sub> regulation of stomatal conductance: advances and  
1047 open questions. *Trends Plant Sci.* 2016 Jan;21(1):16–30.

1048 46. Bansal KC, Viret JF, Haley J, Khan BM, Schantz R, Bogorad L. Transient expression from  
1049 cab-m1 and rbcS-m3 promoter sequences is different in mesophyll and bundle sheath cells  
1050 in maize leaves. *Proc Natl Acad Sci.* 1992 Apr 15;89(8):3654–8.

1051 47. Viret JF, Mabrouk Y, Bogorad L. Transcriptional photoregulation of cell-type-preferred  
1052 expression of maize rbcS-m3: 3' and 5' sequences are involved. *Proc Natl Acad Sci.* 1994  
1053 Aug 30;91(18):8577–81.

1054 48. Lu Z, Marand AP, Ricci WA, Ethridge CL, Zhang X, Schmitz RJ. The prevalence, evolution  
1055 and chromatin signatures of plant regulatory elements. *Nat Plants.* 2019 Dec;5(12):1250–9.

1056 49. Taniguchi M, Izawa K, Ku MSB, Lin JH, Saito H, Ishida Y, et al. The Promoter for the Maize  
1057 C4 Pyruvate,orthophosphate Dikinase Gene Directs Cell- and Tissue-Specific Transcription  
1058 in Transgenic Maize Plants. *Plant Cell Physiol.* 2000 Jan 1;41(1):42–8.

1059 50. Heimann L, Horst I, Perduns R, Dreesen B, Offermann S, Peterhansel C. A Common  
1060 Histone Modification Code on C4 Genes in Maize and Its Conservation in Sorghum and  
1061 *Setaria italica*. *Plant Physiol.* 2013 May 1;162(1):456–69.

1062 51. Paterson AH, Bowers JE, Bruggmann R, Dubchak I, Grimwood J, Gundlach H, et al. The  
1063 Sorghum bicolor genome and the diversification of grasses. *Nature.* 2009 Jan  
1064 29;457(7229):551–6.

1065 52. Maher KA, Bajic M, Kajala K, Reynoso M, Pauluzzi G, West DA, et al. Profiling of  
1066 Accessible Chromatin Regions across Multiple Plant Species and Cell Types Reveals  
1067 Common Gene Regulatory Principles and New Control Modules. *Plant Cell.* 2018  
1068 Jan;30(1):15–36.

1069 53. Yanagisawa S. Dof1 and Dof2 transcription factors are associated with expression of  
1070 multiple genes involved in carbon metabolism in maize. *Plant J.* 2000;21(3):281–8.

1071 54. Perduns R, Horst-Niessen I, Peterhansel C. Photosynthetic Genes and Genes Associated  
1072 with the C4 Trait in Maize Are Characterized by a Unique Class of Highly Regulated Histone  
1073 Acetylation Peaks on Upstream Promoters. *Plant Physiol.* 2015 Aug 1;168(4):1378–88.

1074 55. Emms DM, Covshoff S, Hibberd JM, Kelly S. Independent and Parallel Evolution of New  
1075 Genes by Gene Duplication in Two Origins of C4 Photosynthesis Provides New Insight into  
1076 the Mechanism of Phloem Loading in C4 Species. *Mol Biol Evol.* 2016 Jul;33(7):1796–806.

1077 56. Yan H, Mendieta JP, Zhang X, Marand AP, Liang Y, Luo Z, et al. Evolution of cell-type-  
1078 specific accessible chromatin regions and the cis-regulatory elements that drive lineage-  
1079 specific innovation [Internet]. bioRxiv; 2024 [cited 2024 Jan 13]. p. 2024.01.08.574753.  
1080 Available from: <https://www.biorxiv.org/content/10.1101/2024.01.08.574753v1>

1081 57. Swift J, Luginbuehl LH, Schreier T, Donald RM, Lee T, Nery J, et al. Single nuclei  
1082 sequencing reveals C4 photosynthesis is based on rewiring of ancestral cell identity  
1083 networks [Internet]. bioRxiv; 2023 [cited 2023 Oct 31]. p. 2023.10.26.562893. Available  
1084 from: <https://www.biorxiv.org/content/10.1101/2023.10.26.562893v1>

1085 58. Studer AJ, Schnable JC, Weissmann S, Kolbe AR, McKain MR, Shao Y, et al. The draft  
1086 genome of the C3 panicoid grass species *Dichanthelium oligosanthes*. *Genome Biol.* 2016  
1087 Oct 28;17(1):223.

1088 59. Chen Z, Debernardi JM, Dubcovsky J, Gallavotti A. The combination of morphogenic  
1089 regulators BABY BOOM and GRF-GIF improves maize transformation efficiency [Internet].  
1090 *Plant Biology*; 2022 Sep [cited 2024 Jan 2]. Available from:  
1091 <http://biorxiv.org/lookup/doi/10.1101/2022.09.02.506370>

1092 60. Ciren D, Zebell S, Lippman ZB. Extreme restructuring of cis-regulatory regions controlling a  
1093 deeply conserved plant stem cell regulator [Internet]. bioRxiv; 2023 [cited 2024 Jan 2]. p.  
1094 2023.12.20.572550. Available from:  
1095 <https://www.biorxiv.org/content/10.1101/2023.12.20.572550v1>

1096 61. Liu L, Gallagher J, Arevalo ED, Chen R, Skopelitis T, Wu Q, et al. Enhancing grain-yield-

1097 related traits by CRISPR–Cas9 promoter editing of maize CLE genes. *Nat Plants*. 2021  
1098 Mar;7(3):287–94.

1099 62. Rodríguez-Leal D, Lemmon ZH, Man J, Bartlett ME, Lippman ZB. Engineering Quantitative  
1100 Trait Variation for Crop Improvement by Genome Editing. *Cell*. 2017 Oct;171(2):470–480.e8.

1101 63. Tu X, Marand AP, Schmitz RJ, Zhong S. A combinatorial indexing strategy for low-cost  
1102 epigenomic profiling of plant single cells. *Plant Commun*. 2022 Jul 11;3(4):100308.

1103 64. Hufford MB, Seetharam AS, Woodhouse MR, Chougule KM, Ou S, Liu J, et al. De novo  
1104 assembly, annotation, and comparative analysis of 26 diverse maize genomes. *Science*.  
1105 2021 Aug 6;373(6555):655–62.

1106 65. Liu J, Seetharam AS, Chougule K, Ou S, Swentowsky KW, Gent JI, et al. Gapless assembly  
1107 of maize chromosomes using long-read technologies. *Genome Biol*. 2020 May  
1108 20;21(1):121.

1109 66. Goodstein DM, Shu S, Howson R, Neupane R, Hayes RD, Fazo J, et al. Phytozome: a  
1110 comparative platform for green plant genomics. *Nucleic Acids Res*. 2012 Jan;40(Database  
1111 issue):D1178–86.

1112 67. Martin M. Cutadapt removes adapter sequences from high-throughput sequencing reads.  
1113 *EMBnet.journal*. 2011 May 2;17(1):10–2.

1114 68. Li H, Durbin R. Fast and accurate short read alignment with Burrows–Wheeler transform.  
1115 *Bioinformatics*. 2009 Jul 15;25(14):1754–60.

1116 69. Danecek P, Bonfield JK, Liddle J, Marshall J, Ohan V, Pollard MO, et al. Twelve years of  
1117 SAMtools and BCFtools. *GigaScience*. 2021 Feb 1;10(2):gfab008.

1118 70. Picard Tools - By Broad Institute [Internet]. [cited 2024 Jan 4]. Available from:  
1119 <http://broadinstitute.github.io/picard/>

1120 71. McInnes L, Healy J, Melville J. UMAP: Uniform Manifold Approximation and Projection for  
1121 Dimension Reduction [Internet]. arXiv; 2020 [cited 2022 Dec 19]. Available from:  
1122 <http://arxiv.org/abs/1802.03426>

1123 72. Stewart GW. On the Early History of the Singular Value Decomposition. *SIAM Rev*.  
1124 1993;35(4):551–66.

1125 73. Blondel VD, Guillaume JL, Lambiotte R, Lefebvre E. Fast unfolding of communities in large  
1126 networks. *J Stat Mech Theory Exp*. 2008 Oct;2008(10):P10008.

1127 74. Wolock SL, Lopez R, Klein AM. Scrublet: Computational Identification of Cell Doublets in  
1128 Single-Cell Transcriptomic Data. *Cell Syst*. 2019 Apr;8(4):281–291.e9.

1129 75. Korsunsky I, Millard N, Fan J, Slowikowski K, Zhang F, Wei K, et al. Fast, sensitive and  
1130 accurate integration of single-cell data with Harmony. *Nat Methods*. 2019 Dec;16(12):1289–  
1131 96.

1132 76. Korsunsky I, Nathan A, Millard N, Raychaudhuri S. Presto scales Wilcoxon and auROC  
1133 analyses to millions of observations [Internet]. *Bioinformatics*; 2019 May [cited 2023 Dec  
1134 28]. Available from: <http://biorxiv.org/lookup/doi/10.1101/653253>

1135 77. Love MI, Huber W, Anders S. Moderated estimation of fold change and dispersion for RNA-  
1136 seq data with DESeq2. *Genome Biol*. 2014 Dec 5;15(12):550.

1137 78. Zhang Y, Liu T, Meyer CA, Eeckhoute J, Johnson DS, Bernstein BE, et al. Model-based  
1138 analysis of ChIP-Seq (MACS). *Genome Biol*. 2008;9(9):R137.

1139 79. Zhang K, Hocker JD, Miller M, Hou X, Chiou J, Poirion OB, et al. A single-cell atlas of  
1140 chromatin accessibility in the human genome. *Cell*. 2021 Nov 24;184(24):5985–6001.e19.

1141 80. Domcke S, Hill AJ, Daza RM, Cao J, O'Day DR, Pliner HA, et al. A human cell atlas of fetal  
1142 chromatin accessibility. *Science* [Internet]. 2020 Nov 13 [cited 2020 Nov 12];370(6518).  
1143 Available from: <https://science.sciencemag.org/content/370/6518/eaba7612>

1144 81. Quinlan AR, Hall IM. BEDTools: a flexible suite of utilities for comparing genomic features.  
1145 *Bioinformatics*. 2010 Mar 15;26(6):841–2.

1146 82. Camacho C, Coulouris G, Avagyan V, Ma N, Papadopoulos J, Bealer K, et al. BLAST+:  
1147 architecture and applications. *BMC Bioinformatics*. 2009 Dec 15;10:421.

1148 83. Grant CE, Bailey TL. XSTREME: Comprehensive motif analysis of biological sequence  
1149 datasets [Internet]. bioRxiv; 2021 [cited 2024 Jan 23]. p. 2021.09.02.458722. Available  
1150 from: <https://www.biorxiv.org/content/10.1101/2021.09.02.458722v1>

1151 84. Bailey TL, Johnson J, Grant CE, Noble WS. The MEME Suite. Nucleic Acids Res. 2015 Jul  
1152 1;43(W1):W39–49.

1153 85. Bioconductor [Internet]. [cited 2024 Jan 23]. universalmotif. Available from:  
1154 <http://bioconductor.org/packages/universalmotif/>

1155 86. Bioconductor [Internet]. [cited 2024 Feb 1]. motifmatchr. Available from:  
1156 <http://bioconductor.org/packages/motifmatchr/>

1157 87. Castro-Mondragon JA, Riudavets-Puig R, Rauluseviciute I, Lemma RB, Turchi L, Blanc-  
1158 Mathieu R, et al. JASPAR 2022: the 9th release of the open-access database of  
1159 transcription factor binding profiles. Nucleic Acids Res. 2022 Jan 7;50(D1):D165–73.

1160 88. Rauluseviciute I, Riudavets-Puig R, Blanc-Mathieu R, Castro-Mondragon JA, Ferenc K,  
1161 Kumar V, et al. JASPAR 2024: 20th anniversary of the open-access database of  
1162 transcription factor binding profiles. Nucleic Acids Res. 2024 Jan 5;52(D1):D174–82.

1163 89. Zenker S, Wulf D, Meierhenrich A, Becker S, Eisenhut M, Stracke R, et al. Transcription  
1164 factors operate on a limited vocabulary of binding motifs in *Arabidopsis thaliana* [Internet].  
1165 2023 [cited 2024 May 3]. Available from:  
1166 <http://biorxiv.org/lookup/doi/10.1101/2023.08.28.555073>